NASA Technical Memorandum 87641

Low-Speed Wind-Tunnel Investigation of the Effect of Strakes and Nose Chines on Lateral-Directional Stability of a Fighter Configuration

Jay M. Brandon

FEBRUARY 1986

NASA

NASA Technical Memorandum 87641

Low-Speed Wind-Tunnel Investigation of the Effect of Strakes and Nose Chines on Lateral-Directional Stability of a Fighter Configuration

Jay M. Brandon
Langley Research Center
Hampton, Virginia

National Aeronautics
and Space Administration

Scientific and Technical Information Branch

1986

Summary

A series of low-speed static wind-tunnel force tests were conducted on a 0.15-scale model of a modern high-performance fighter aircraft. The tests identified sources of lateral-directional instabilities and investigated the use of nose chines to enhance stability at high angles of attack.

Results of this investigation showed that the strake was the major contributor to directional instability. The destabilizing forces were created by two mechanisms: (1) adverse flow in the region of the vertical tail, and (2) forces generated on the fuselage ahead of the center of gravity. Properly designed nose chines effectively negated the adverse flow near the vertical tail and created stabilizing forces on the forebody in the range of the stall angle of attack.

Introduction

Most current high-performance fighter airplanes exhibit some degree of lateral-directional instability at high angles of attack. This instability can be manifested in various dynamic phenomena, such as yaw divergence or wing rock, which lead to inadvertent spins or other departures from controlled flight. These adverse characteristics can preclude effective maneuvering at high-angle-of-attack conditions, where maneuvering capability can be very advantageous in air combat. (See ref. 1.) There is a broad research program under way at NASA to further the understanding of high-angle-of-attack aerodynamics, which determine stability characteristics, and to develop design guidelines for future aircraft to ensure desirable flying characteristics. The current program builds upon and extends previous research efforts, which were directed toward specific designs with variations in key configuration components such as forebody shapes, strake design, and tail placement. (See refs. 2 through 8.)

In the present study, exploratory stability studies were conducted on a subscale model of a modern single-engine fighter airplane. The objectives of the test program were to provide fundamental high-angle-of-attack stability information for use in improving the lateral-directional stability characteristics of the subject configuration and to establish design guidelines for future fighter aircraft. Specific points of interest in the study included identification of configurational components that cause high-angle-of-attack instabilities and identification of modifications that could be made to improve stability levels. Particular emphasis was placed on the modification of the forebody aerodynamics by adding nose chines to the existing nose.

Symbols

All longitudinal aerodynamic coefficients are referenced to the wind-axis system, and all lateral-directional data are referenced to the body-axis system. All force-data test results were obtained with the moment reference center at 35-percent of the wing aerodynamic chord.

b	wing span, ft
$\bar{c}$	mean aerodynamic chord, ft
C_L	lift coefficient, $\frac{\text{Lift}}{qS}$
C_l	rolling-moment coefficient, $\frac{\text{Rolling moment}}{qSb}$
C_{l_β}	$\frac{\partial C_l}{\partial \beta}$, per degree
C_m	pitching-moment coefficient, $\frac{\text{Pitching moment}}{qS\bar{c}}$
C_n	yawing-moment coefficient, $\frac{\text{Yawing moment}}{qSb}$
C_{n_β}	$\frac{\partial C_n}{\partial \beta}$, per degree
C_Y	side-force coefficient, $\frac{\text{Side force}}{qS}$
C_{Y_β}	$\frac{\partial C_Y}{\partial \beta}$, per degree
q	free-stream dynamic pressure, lb/ft^2
S	reference wing area, ft^2
α	angle of attack, deg
β	angle of sideslip, deg
ΔC_{l_β}	lateral stability effectiveness, per degree
ΔC_{n_β}	directional stability effectiveness, per degree
δ_h	horizontal tail incidence, positive with trailing edge down, deg
δ_r	rudder deflection angle, positive with trailing edge left, deg

Model and Tests

A three-view sketch of the model used in the tests is shown in figure 1. Geometric characteristics are listed in table I. The model was a 0.15-scale model of the full-scale General Dynamics YF-16 airplane. Several modifications to the airplane geometry were tested. These modifications are shown in figures 2

and 3. Figure 2 shows strake variations tested. Figure 3 is a comparison of various nose chines tested.

The wind-tunnel tests were conducted at the Langley Research Center in a low-speed wind tunnel with an octagonal cross section of 12 ft. The model was sting mounted on a six-component, internally mounted, strain-gauge balance. The engine inlet and exit were open to allow airflow through the model during the tests, which were conducted at a tunnel speed of 65 ft/sec to correspond with a Reynolds number of 0.68×10^6 based on the wing mean aerodynamic chord. No corrections were made for blockage, buoyancy, or internal aerodynamics. Data were obtained through angle-of-attack and angle-of-sideslip ranges of 0° to 55° and −10° to 10°, respectively.

Results and Discussion

Longitudinal Characteristics

Basic configuration. The basic configuration is shown in figure 1. The leading-edge flap is deflected 25° leading-edge down to represent low-speed flight geometry. Although the emphasis in this study was on the lateral-directional characteristics, longitudinal characteristics are presented for reference purposes. Figure 4 shows lift and pitching-moment data for the basic configuration. The pitching-moment data show that the basic configuration is slightly unstable in pitch, about 3.5-percent unstable static margin at $\alpha = 25°$, and the pitch instability increases abruptly at $\alpha = 37°$. Configuration component effects on longitudinal characteristics are shown in figure 5. The data in figure 5 indicate that the strake produces a large destabilizing increment in pitching moment above $\alpha = 12°$. Addition of the horizontal tail ($\delta_h = 0°$) significantly reduces the pitching moment and increases the maximum lift of the wing-body-strake combination.

Strake configurations. Reductions in strake size were made to assess the effect of the strake on stability characteristics. The baseline strake was replaced by an uncambered strake with a similar planform. The flat strake was systematically cut at the locations shown in figure 2; this resulted in notched strakes, each with less area than the original. Although a substantial performance difference may exist between strakes of differing cross-sectional geometries, these differences would not be expected to significantly alter data trends obtained by strake size reductions. Figure 6 shows that each reduction of strake size resulted in sizeable reductions in maximum lift coefficient and improved pitch stability. The large degradation of maximum lift coefficient associated with reduction in strake size is a severe, and probably unacceptable, performance penalty.

Nose-chine configurations. Several nose chines (fig. 3) were tested as additions to the baseline configuration. The chines tested were 1.5 and 3 in. wide (full scale) and, because of their small size, had very little effect on longitudinal stability. (See fig. 7.)

Lateral-Directional Characteristics

Basic configuration. The lateral-directional characteristics of the basic configuration are shown in figure 8. The values of directional stability C_{n_β} show a severe degradation between $\alpha = 25°$ and $\alpha = 45°$, and the configuration is directionally unstable at angles of attack greater than 29°. The C_{l_β} values indicate that the configuration has stable static lateral characteristics throughout the angle-of-attack range.

To identify the component sources of the lateral-directional stability characteristics, a series of component buildup tests were made with various combinations of wing, body, canopy, strake, and tails, and the results of the tests are presented in figure 9. The data show that above $\alpha = 33°$, the body alone is directionally stable. Adding the strake and the canopy decreases the high-angle-of-attack directional stability. The vertical tail adds a positive increment to C_{n_β} at angles of attack below 35°, but is destabilizing at higher angles of attack. The vertical tail provides a stabilizing increment to C_{l_β} which results in the configuration having positive lateral stability over the entire angle-of-attack range tested.

Figure 10 presents the effect of the strake on lateral and directional stability. The values of lateral and directional stability effectiveness, ΔC_{l_β} and ΔC_{n_β}, respectively, are computed as the difference of the values of C_{l_β} or C_{n_β} with and without the configuration component for which effectiveness is being computed. The small values of ΔC_{n_β} below 30° in figure 10 indicate that the strake has little influence on directional stability at low angles of attack. At higher values of α, however, the strake provides a very large destabilizing increment in directional stability. The contributions of the vertical tail to lateral-directional stability are shown in figure 11. The data indicate that the tail provides a nearly constant stable increment to C_{n_β} until $\alpha = 26°$. The increment degrades rapidly as angle of attack is further increased. Above $\alpha = 32°$, the vertical tail is directionally destabilizing. The vertical tail contributes a stable increment to C_{l_β} for most of the angle-of-attack range.

The measured rudder effectiveness is shown in figure 12. The data indicate that the rudder maintains a near-constant level of effectiveness to 35° angle of attack and provides some control power through the entire angle-of-attack range tested. These results suggest that the dramatic reduction in vertical-tail contribution to directional stability between $\alpha = 26°$ and $\alpha = 35°$ is not caused by a reduction of dynamic pressure at the vertical tail, but is associated with adverse sidewash effects. Above 35°, a possibility that the vertical tail is being blanketed by wing wake exists. The canopy effect on lateral-directional stability is shown in figure 13. The canopy is destabilizing directionally at all angles of attack. In the angle-of-attack range between 25° and 50°, the canopy provides a stabilizing increment to C_{l_β}.

Figures 14 and 15 illustrate the relationship of the various configuration components to other key components. The figures show the effect of the strake on lateral-directional stability for: (1) the complete basic configuration; (2) the configuration with the vertical tail removed; and (3) the configuration with the canopy removed. The data show a large destabilizing increment in C_{n_β} caused by the interaction of the strake and vertical tail in the 30° to 50° angle-of-attack range. Figure 15 shows that interactions between the strake, vertical tail, and canopy result in stabilizing increments in C_{l_β} in the 30° to 50° angle-of-attack range.

A commonly used method for analysis of directional stability characteristics involves correlating C_{Y_β} with C_{n_β}. When the two parameters have opposite signs, this suggests that the forces producing the yawing moments are predominantly acting behind the center of gravity. Conversely, when C_{Y_β} and C_{n_β} have the same polarity, it is indicative of the forces acting in front of the center of gravity. The values of C_{n_β} and C_{Y_β} are plotted in figure 16 for the model with the body and canopy only. As expected, the unstable values of C_{n_β} at low angles of attack are caused by the area ahead of the center of gravity. Between $\alpha = 25°$ and $\alpha = 35°$, the instability is aggravated by afterbody destabilizing contributions. Above $\alpha = 45°$, the afterbody becomes stabilizing. Addition of the strake (fig. 17) reduces the favorable fuselage effect at angles of attack above 40°. Results for the basic configuration (fig. 18) show that the vertical tail is the dominant component in the low-angle-of-attack range. Above $\alpha = 30°$, destabilizing forces ahead of the center of gravity dominate. Figure 19 shows that the configuration with the strake removed exhibits a significantly lower level of directional instability above $\alpha = 29°$ than the basic configuration. Thus, it appears that the strake degrades the directional stability of the configuration in two ways: (1) adverse interaction with the vertical tail; and (2) magnification of forebody destabilizing forces.

Strake configurations. Past studies (e.g., ref. 6) with similar configurations have indicated a correlation between strake geometry and directional stability characteristics in the region around the stall. The YF-16 has a strake which is highly blended into the fuselage. To explore strake geometry effects, this strake was replaced by a flat-plate strake with a planform similar to that of the original. A comparison of the directional stability for the flat-strake and baseline configurations is shown in figure 20. The closeness of the values of C_{n_β} for the two configurations indicates that the thickness, cambering, and blending of the baseline strake have little influence on static directional stability. The values of C_{l_β} apparently are more dependent on strake cross-sectional shape and do not compare as well; however the major purpose for using the flat strakes was to study effects on directional stability. The flat strake was systematically cut at the locations shown in figure 2 and resulted in notched strakes, each with less area than the original. Figure 21 shows the effect of the reduction in strake size on lateral-directional characteristics. Each progressive reduction in strake area increases high-angle-of-attack directional stability, particularly above $\alpha = 30°$. To a lesser degree, lateral stability C_{l_β} is also affected by strake size.

Nose chine configurations. The previous data indicate that forces ahead of the center of gravity dominate the directional stability characteristics exhibited by this configuration at high angles of attack. Since the major contributor to the directional stability at high angles of attack was the area ahead of the center of gravity, the forebody was modified by the addition of nose chines. Nose-chine width and length effects were investigated with the use of several nose chines. (See fig. 3.) As reported in reference 7, for the chines to have much effect on the aerodynamic characteristics of the model, they must extend in front of the nose. The effects of the various chines on lateral-directional stability derivatives are summarized in figures 22 and 23.

1.5-in. chines. Nose chines 1 through 4 (fig. 3) had a full-scale width of 1.5 in. Chine 1 was modified to give chines 2, 3, and 4. The effect of adding to the length of the chine ahead of the nose is seen by comparing results from chines 1, 2, and 3 in figures 22(a) and 23(a). Chines 2 and 3 each successively extended

farther in front of the nose. The increases in static stability (both C_{n_β} and C_{l_β}) from chine 1 to chine 2 are significant, but a further increase to the length of chine 3 showed little improvement. All the 1.5-in. chine configurations tested significantly increased the range of angle of attack over which the model retained static lateral-directional stability.

Chine 4. The chine-4 configuration was made by adding a rounded aft end to chine 2. This chine increased the range of angle of attack where C_{n_β} remained positive to beyond 47°. Roll stability was not degraded significantly compared with chine 2. The addition of chine 4 increased the stable lateral-directional range over the basic configuration by 18° angle of attack. (See figs. 22(a) and 23(a).) The differences in C_{n_β} and C_{l_β} for chine 2 and C_{n_β} and C_{l_β} for chine 4 illustrate the highly sensitive nature of forebody geometry effects on lateral-directional stability at high angles of attack.

To investigate the source of the directional stability improvement, several comparisons between the chine-4 configuration and the basic configuration were made. Figure 24 shows a comparison of the vertical-tail effectiveness with and without the chine. The large increase in vertical-tail effectiveness is caused by the addition of the chine in the angle-of-attack range between 20° and 30°. This increase in tail effectiveness is probably caused by the interaction of the strake and chine vortices as they propagate toward the tail. A comparison of the effect on stability of the strake with and without the nose chine is shown in figure 25. The addition of the nose chine reduced the destabilizing effect of the strake at high angles of attack. Figure 26 shows C_{n_β} and C_{Y_β} for the chine-4 configuration. This figure indicates that at angles of attack below 31°, the directionally stabilizing forces are acting on the rear of the model. The large stable values of C_{n_β} between $\alpha = 20°$ and $\alpha = 31°$ are apparently a result of the increase in effectiveness of the vertical tail. Comparing these results with the basic configuration (fig. 18) shows that the addition of the chine reversed the unstable contribution of the forward area of the basic configuration from $\alpha = 31°$ to $\alpha = 42°$. The forces ahead of the center of gravity on the basic configuration dominated static directional characteristics above $\alpha = 29°$ in a destabilizing manner. The static directional stability characteristics of the chine-4 configuration at angles of attack between 31° and 42° were also dominated by the forces ahead of the center of gravity. However, the addition of the chine caused these forces to be stabilizing to C_{n_β} in contrast to the basic configuration. As discussed in reference 9, stabilizing forebody contributions to C_{n_β} can also produce unstable yaw-damping characteristics which may negate the improvements in static stability. Additional tests are needed to investigate the effect of this chine on yaw damping and the potential impact on departure susceptibility.

Further investigation of the component contributions to directional stability characteristics are shown in figures 19 and 27 through 29. Figure 27 shows C_{n_β} and C_{Y_β} for the chine-4 configuration without the vertical tail. This plot may be compared with that of figure 28, which shows C_{n_β} and C_{Y_β} for the basic configuration minus the vertical tail. As shown previously, C_{n_β} for the basic configuration remains negative (unstable) throughout the angle-of-attack range. Correlation of C_{n_β} and C_{Y_β} values confirms that the area ahead of the center of gravity is the major destabilizing influence at all angles of attack. The configuration with the chine (fig. 27) is directionally stable from $\alpha = 31°$ to $\alpha = 48°$. Comparison of C_{n_β} and C_{Y_β} values for the two configurations indicates that a vast difference in the flow mechnisms exists. For the chine-4 configuration, the area ahead of the center of gravity provides a stabilizing contribution in the angle-of-attack range from 31° to 42°. Above 48°, the forebody becomes destabilizing. Figures 29 and 19 show C_{n_β} and C_{Y_β} for the chine-4 configuration minus the strake and basic configuration minus the strake, respectively. The chine-4 configuration without the strake (fig. 29) remains directionally stable throughout the angle-of-attack range tested. The basic configuration is unstable above $\alpha = 28°$, primarily because of forces acting on the area ahead of the center of gravity. As discussed previously, the configuration without the strake is not as unstable as the full basic configuration (fig. 18), but the instability arises at about the same angle of attack for each case. The removal of the strake and the addition of the nose chine maintain the tail effectiveness as the major contributor to stability up to $\alpha = 33°$. From $\alpha = 33°$ to $\alpha = 53°$, the forward fuselage area had the dominant stabilizing influence. A large amount of flow interaction between the various configurational components is evident in comparisons of the basic and chine-4 configurations with and without the strake. (See figs. 19 and 29.)

3-in. chines. Several chines of various lengths with a 3-in. full-scale width were tested to assess the effect of chine width and to further investigate the effects of chine length. The results of these tests indicated that the effectiveness of the nose chine in improving lateral-directional stability is very sensitive to the length of the chine. Chine 5 extended

from a point ahead of the nose back to the strake. The length of the chine on the forebody was reduced successively to form chine configurations 6 through 9. The effects of these chines on the lateral-directional stability are seen in figures 22(b) and 23(b). Chine 5 increased the angle-of-attack range for stable C_{n_β} by 19° compared with the basic configuration. A corresponding large loss in lateral stability was also observed. Shortening the chine along the forebody to chine configuration 6 caused a sharp reduction in C_{n_β}, but caused an increase in stable C_{l_β}. A further reduction of chine 6 to produce chine 7 provided an increase in C_{n_β} as well as a substantial improvement in lateral stability. (See following section.) Further chine-length reductions to chines 8 and 9 resulted in large destabilizing increments in C_{l_β}.

Chine 7. Chine 7 has the same length as the 1.5-in. chine 1. Comparison of the two chines in figures 22 and 23 shows that the directional stability is nearly the same with both chines and that lateral stability is slightly greater with the wider nose chine.

Radial position. Significant changes in the effectiveness of forebody chines as a result of radial positioning have been observed in past studies. (See refs. 7 and 8.) Two other radial positions (20° above and below the maximum half-breadth position) were tested using nose chine 7. The results of the test are summarized in figure 30. The figure indicates that the original 0° radial location provided the most favorable static lateral-directional stability characteristics. The −20° radial location produced essentially the same levels of directional and lateral stability as the 0° position. At the higher angle-of-attack range, the directional stability for the chine configuration with the 20° radial location is lower than that for the chine configuration with the 0° radial location. A sharp decrease in the lateral stability parameter, C_{l_β}, for $30° < \alpha < 45°$ is also seen with the chine at the +20° radial location.

Concluding Remarks

A low-speed wind-tunnel study was conducted on a model of a modern high-performance airplane. The study identified some of the sources of the lateral-directional instability exhibited by the configuration at high angles of attack and showed that proper application of forebody chines can significantly improve the static stability of this configuration. The results of the study can be summarized as follows:

1. The wing-body strake is the major contributor to directional instability above an angle of attack of 29°. The wing-body strake degrades the directional stability of the configuration by adverse interaction with the vertical tail and by magnification of forebody destabilizing forces.

2. Reducing the size of the wing-body strake improves directional stability but severely penalizes lift.

3. Proper design and placement of nose chines significantly enhances directional stability with no loss in lift and with very minor effects on pitching moment. In the 20° to 30° angle-of-attack range, the interaction of the chine and wing-body-strake vortices significantly increases vertical-tail effectiveness. At higher angles of attack, the nose chines develop flow characteristics which create statically stabilizing forces on the area ahead of the center of gravity to give the configuration stable directional characteristics up to an angle of attack of 42°.

NASA Langley Research Center
Hampton, VA 23665-5225
December 4, 1985

References

1. Hamilton, William L.; and Skow, Andrew M.: *Operational Utility Survey: Supermaneuverability.* AFWAL-TR-85-3020, U.S. Air Force, Sept. 1984.
2. Carr, Peter C.; and Gilbert, William P.: *Effects of Fuselage Forebody Geometry on Low-Speed Lateral-Directional Characteristics of Twin-Tail Fighter Model at High Angles of Attack.* NASA TP-1592, 1979.
3. Klein, John R.; Walck, Kenneth J.; and Hahne, David E.: Airframe Component Effects on the Aerodynamic Stability and Control Characteristics of a Supersonic Cruise Fighter Aircraft at High Angles of Attack. AIAA-84-2110, Aug. 1984.
4. Skow, A. M.; and Erickson, G. E.: Modern Fighter Aircraft Design for High-Angle-of-Attack Maneuvering. *High Angle-of-Atttack Aerodynamics,* AGARD-LS-121, Dec. 1982, pp. 4-1–4-59.
5. Shrout, Barrett L.; and Covell, Peter F.: *Aerodynamic Characteristics of a Series of Bodies With Variations in Nose Camber.* NASA TP-2206, 1983.
6. Erickson, Gary E.: *Water Tunnel Flow Visualization and Wind Tunnel Data Analysis of the F/A-18.* NASA CR-165859, 1982.
7. Smith, C. W.; Ralston, J. N.; and Mann, H. W.: *Aerodynamic Characteristics of Forebody and Nose Strakes Based on F-16 Wind Tunnel Test Experience. Volume I: Summary and Analysis.* NASA CR-3053, 1979.
8. Erickson, Gary E.; and Gilbert, William P.: Experimental Investigation of Forebody and Wing Leading-Edge Vortex Interactions at High Angles of Attack. *Aerodynamics of Vortical Type Flows in Three Dimensions,* AGARD-CP-342, July 1983, pp. 11-1–11-20.
9. Grafton, Sue B.; Chambers, Joseph R.; and Coe, Paul L., Jr.: *Wind-Tunnel Free-Flight Investigation of a Model of a Spin-Resistant Fighter Configuration.* NASA TN D-7716, 1974.

TABLE I. MODEL GEOMETRIC CHARACTERISTICS

Wing:	
Span, ft	4.35
Area, ft^2	6.30
Mean aerodynamic chord, ft	1.64
Aspect ratio	3.00
Taper ratio	0.23
Sweepback of leading edge, deg	40
Dihedral, deg	0
Incidence, deg	0
Airfoil section	NACA 64A204
Leading-edge flap area, ft^2	0.76
Horizontal tail:	
Area, ft^2	2.36
Movable area (one side), ft^2	0.49
Span, ft	2.62
Aspect ratio	3.19
Taper ratio	0.20
Sweepback of leading edge, deg	40
Dihedral, deg	−10
Vertical tail:	
Area, ft^2	1.23
Span, ft	1.26
Taper ratio	0.44
Root chord, ft	1.35
Tip chord, ft	0.59
Sweepback of leading edge, deg	47.5
Rudder area, ft^2	0.26
Ventral fin:	
Area, ft^2	0.16
Span, ft	0.29
Aspect ratio	0.36
Taper ratio	0.69
Sweepback of leading edge, deg	45
Dihedral, deg	15 outboard

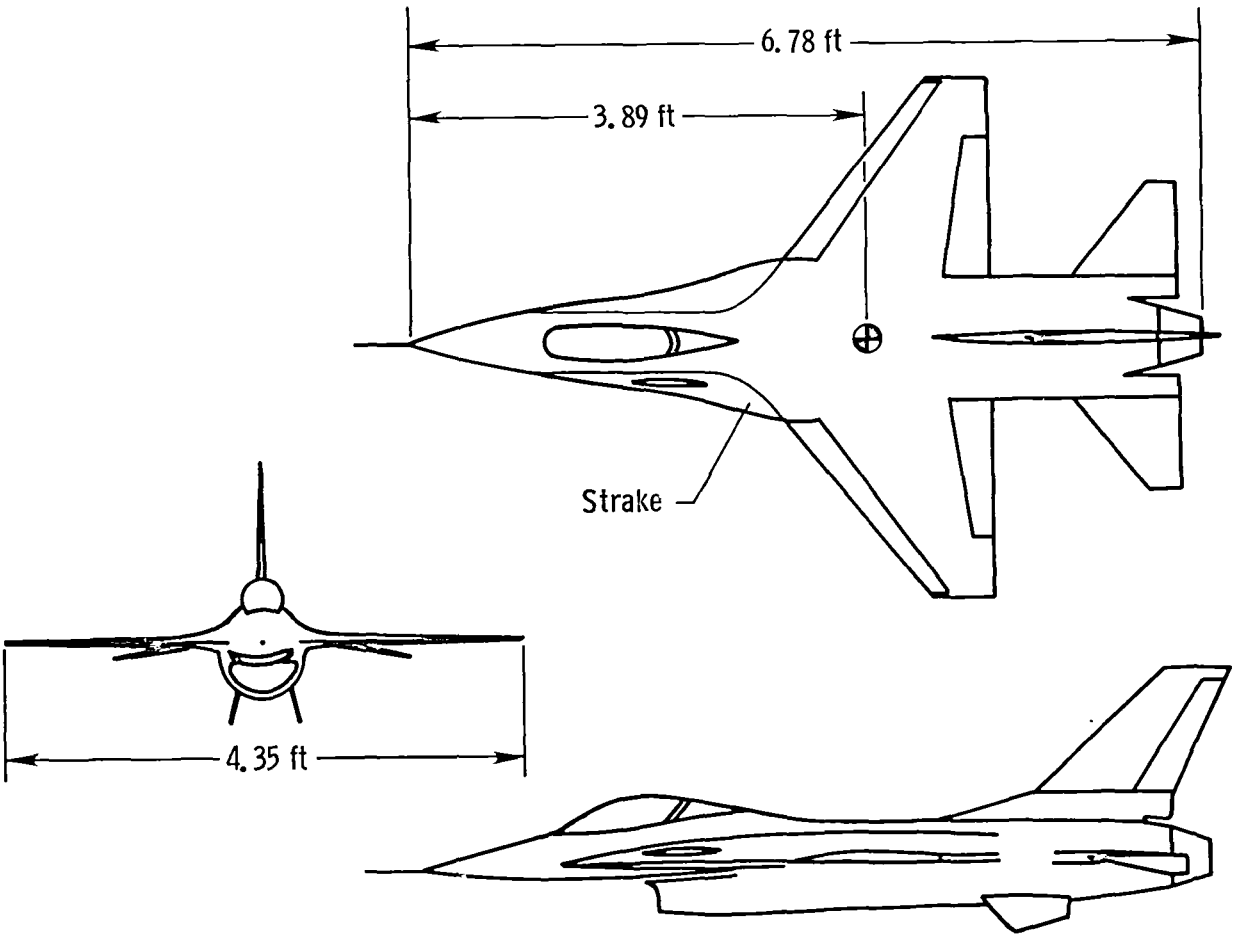

Figure 1. Sketch of model.

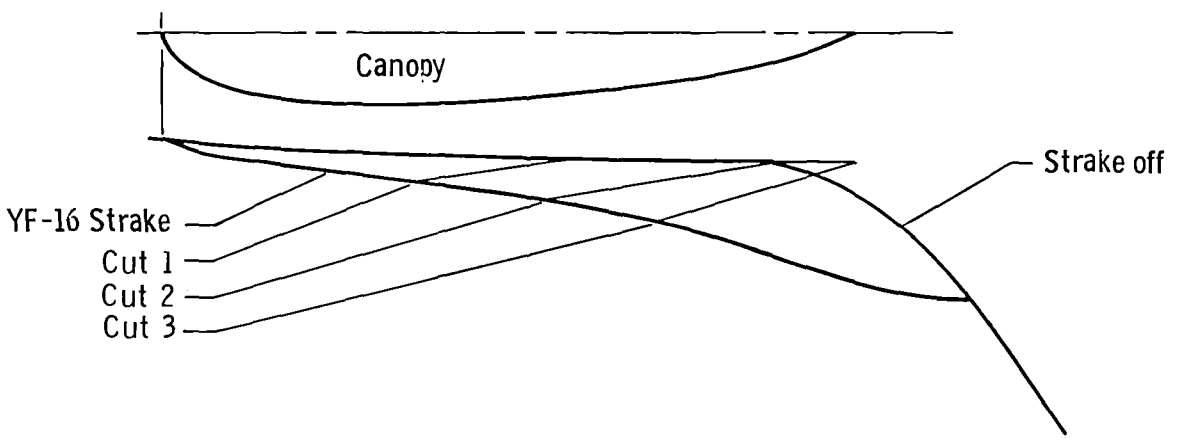

Figure 2. Strake modifications.

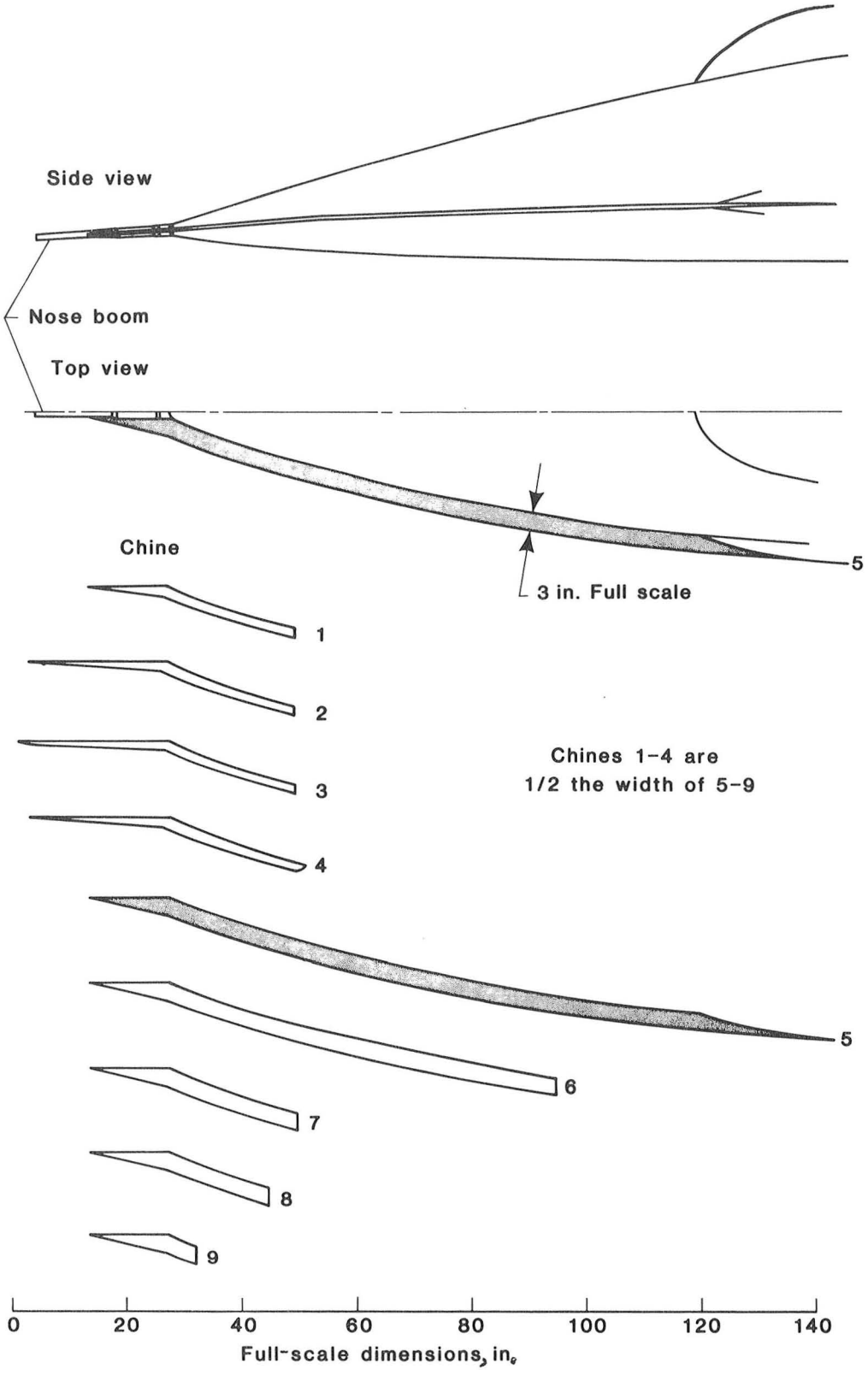

Figure 3. Nose chines tested.

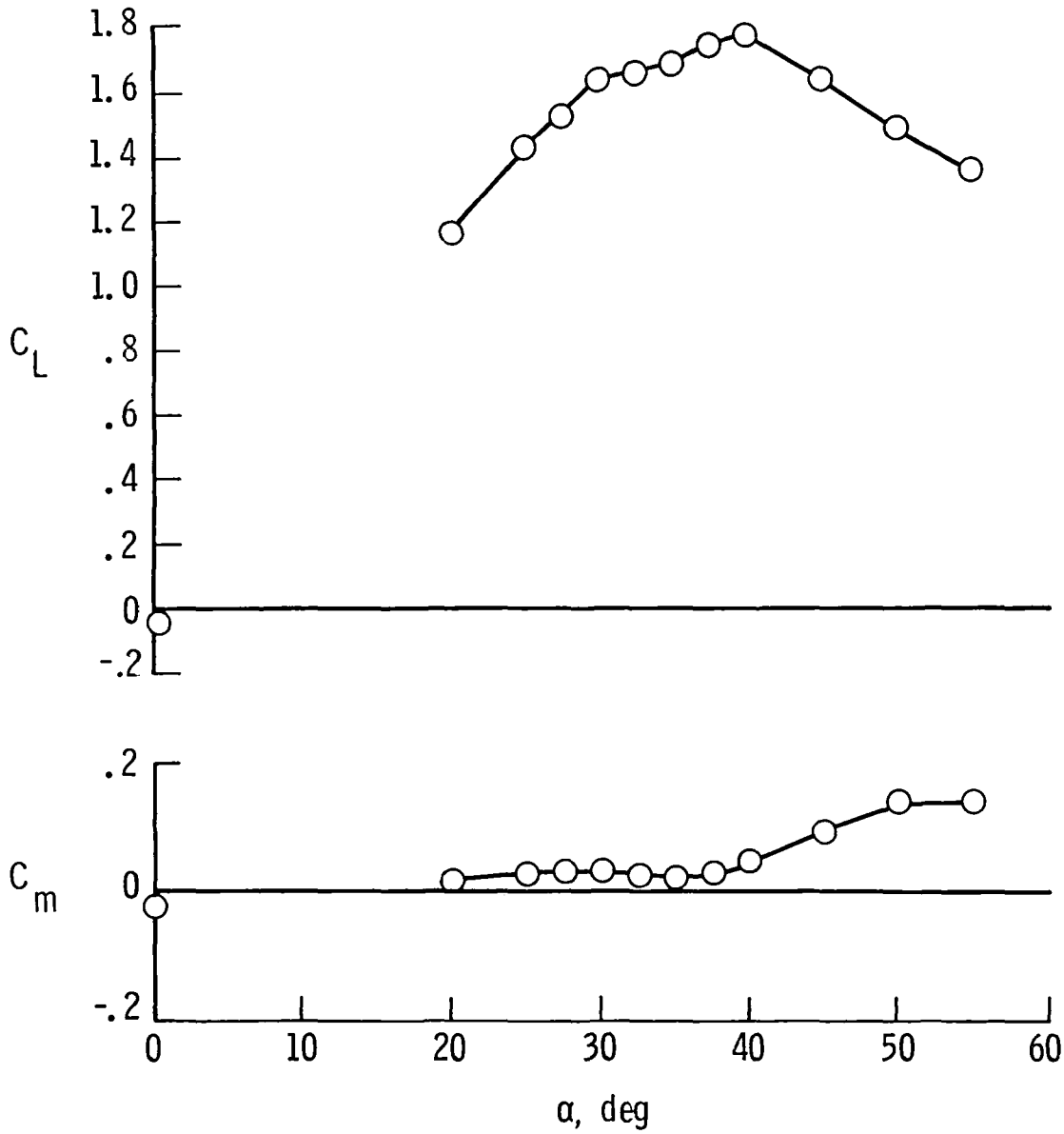

Figure 4. Longitudinal characteristics of basic configuration.

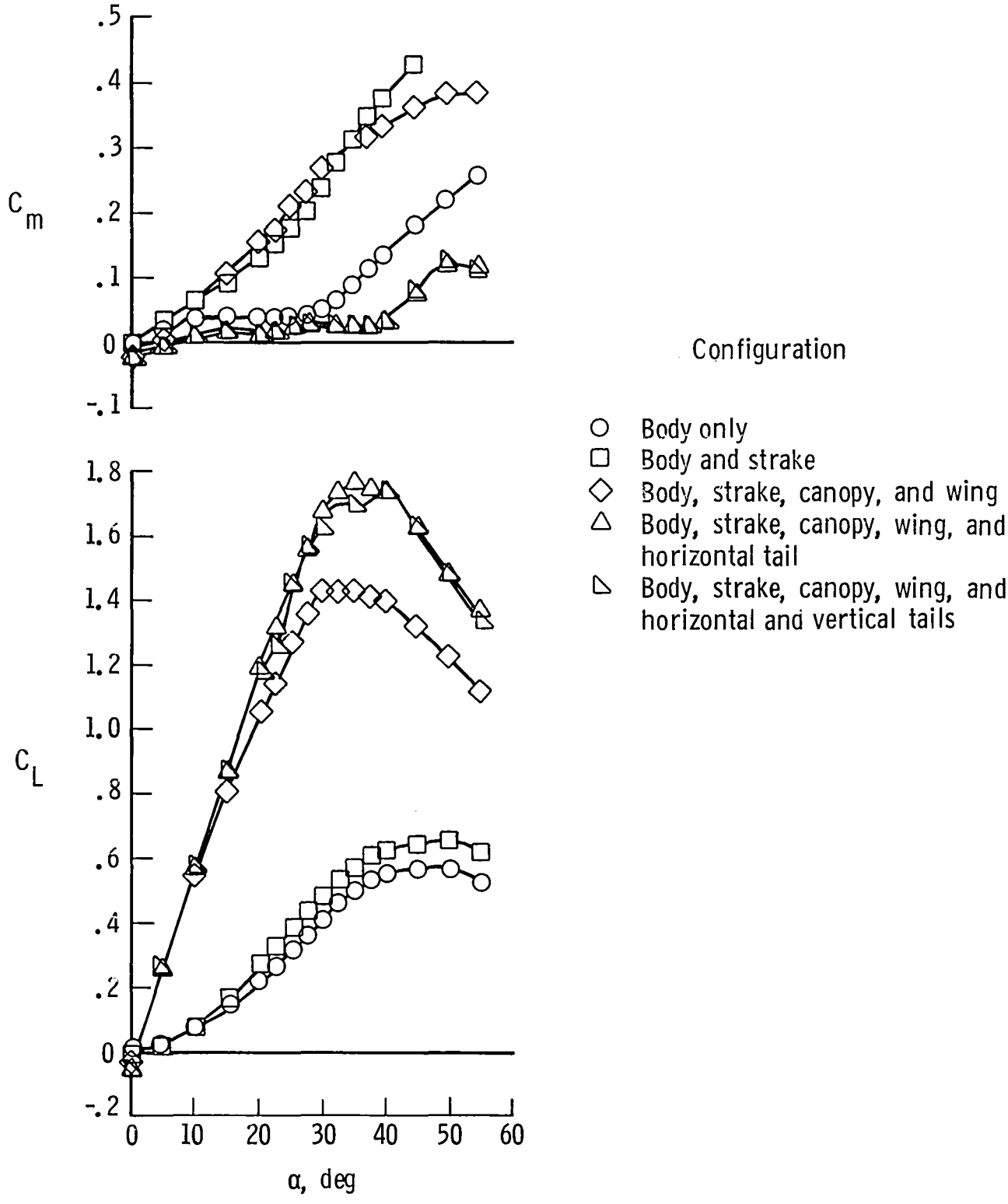

Figure 5. Component effects on longitudinal characteristics.

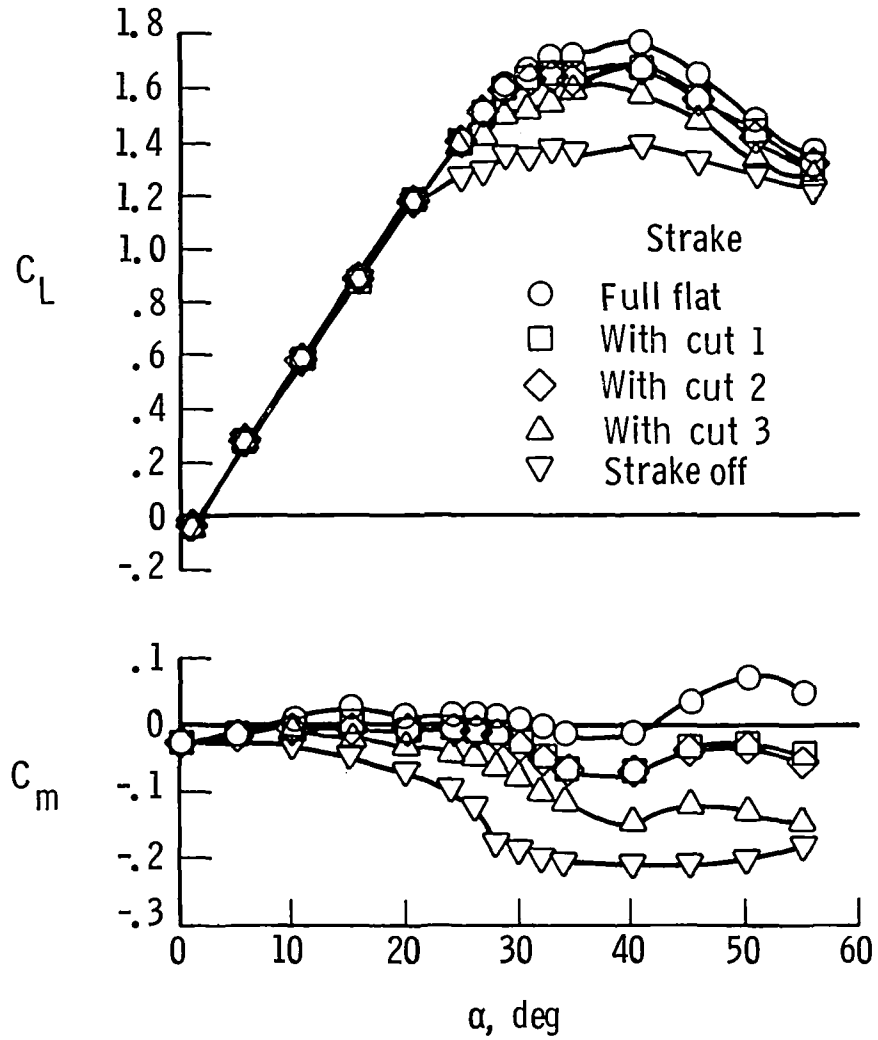

Figure 6. Effect of strake on longitudinal characteristics of basic configuration.

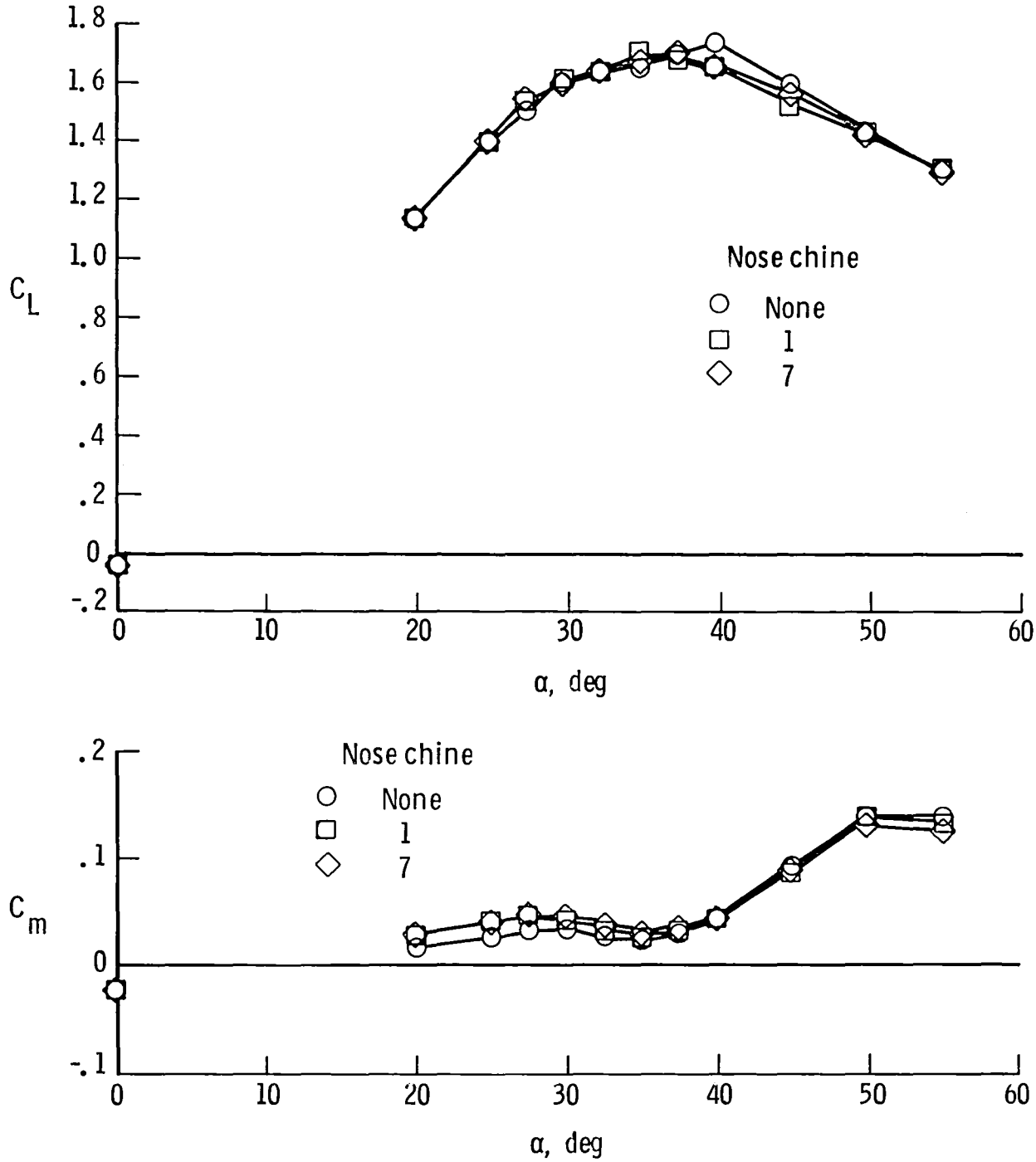

Figure 7. Effect of nose chines on longitudinal characteristics of basic configuration.

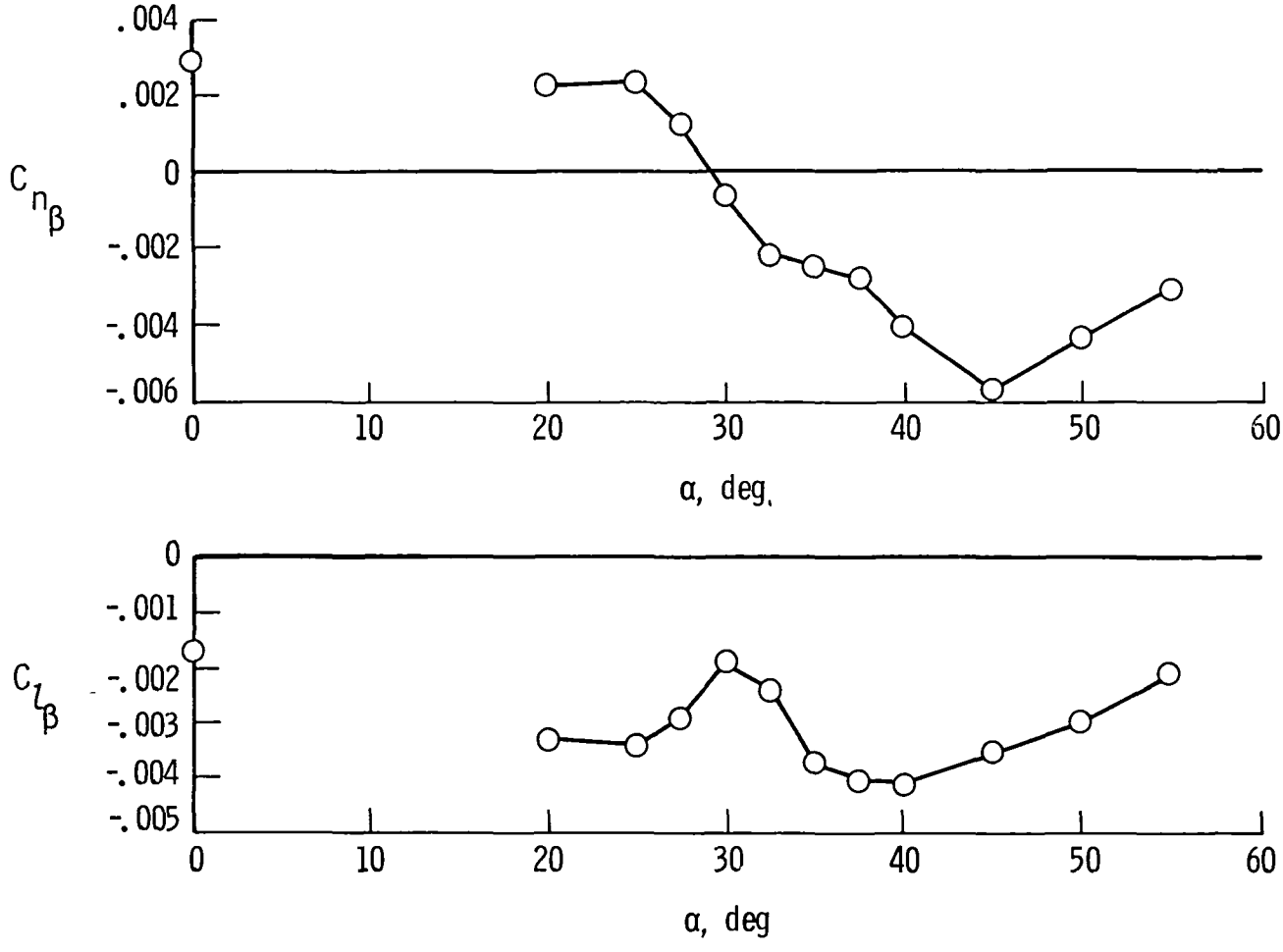

Figure 8. Lateral-directional stability characteristics of basic configuration.

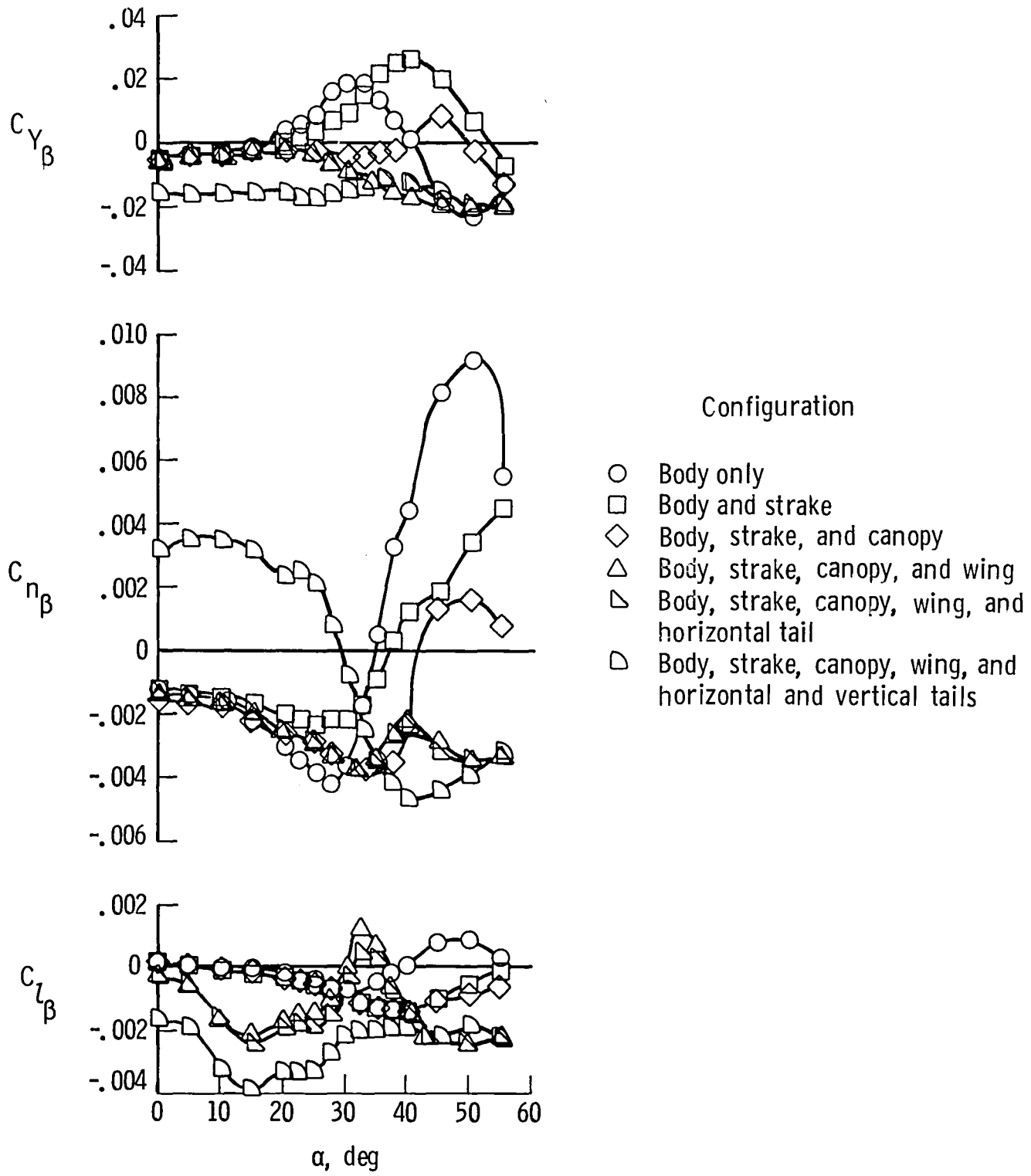

Figure 9. Component effects on lateral-directional stability.

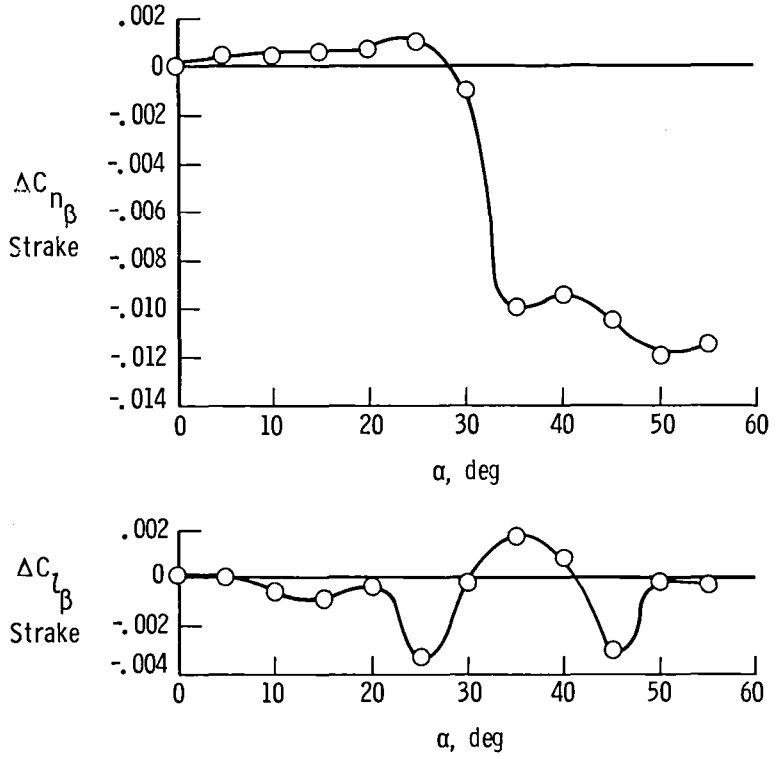

Figure 10. Effect of strake on lateral-directional stability.

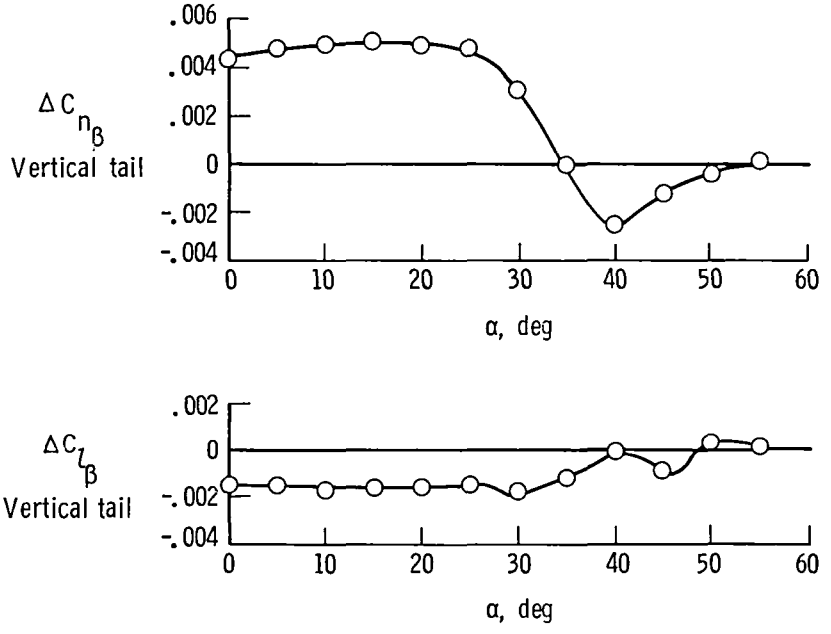

Figure 11. Effect of vertical tail on lateral-directional stability.

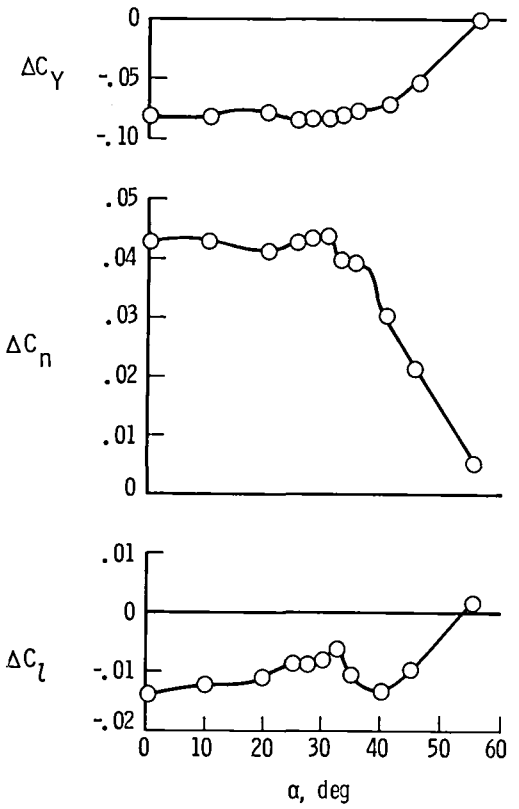

Figure 12. Rudder effectiveness. $\delta_r = -30°$.

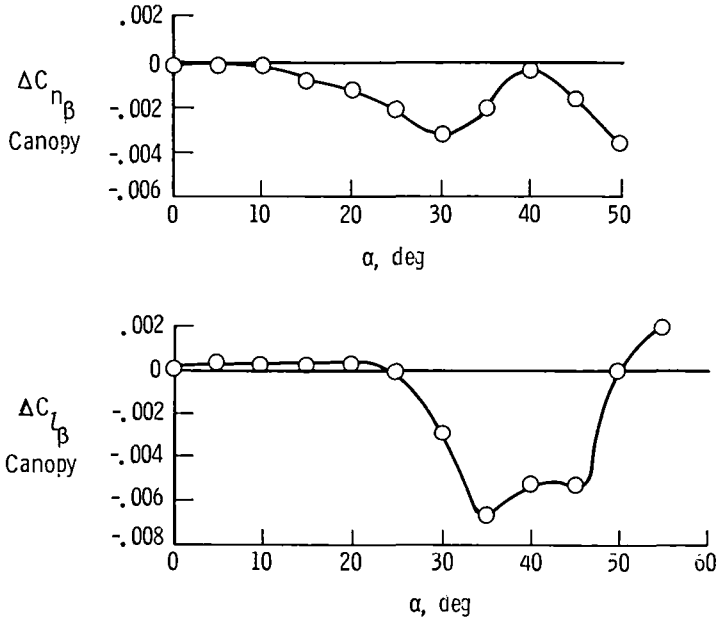

Figure 13. Effect of canopy on lateral-directional stability.

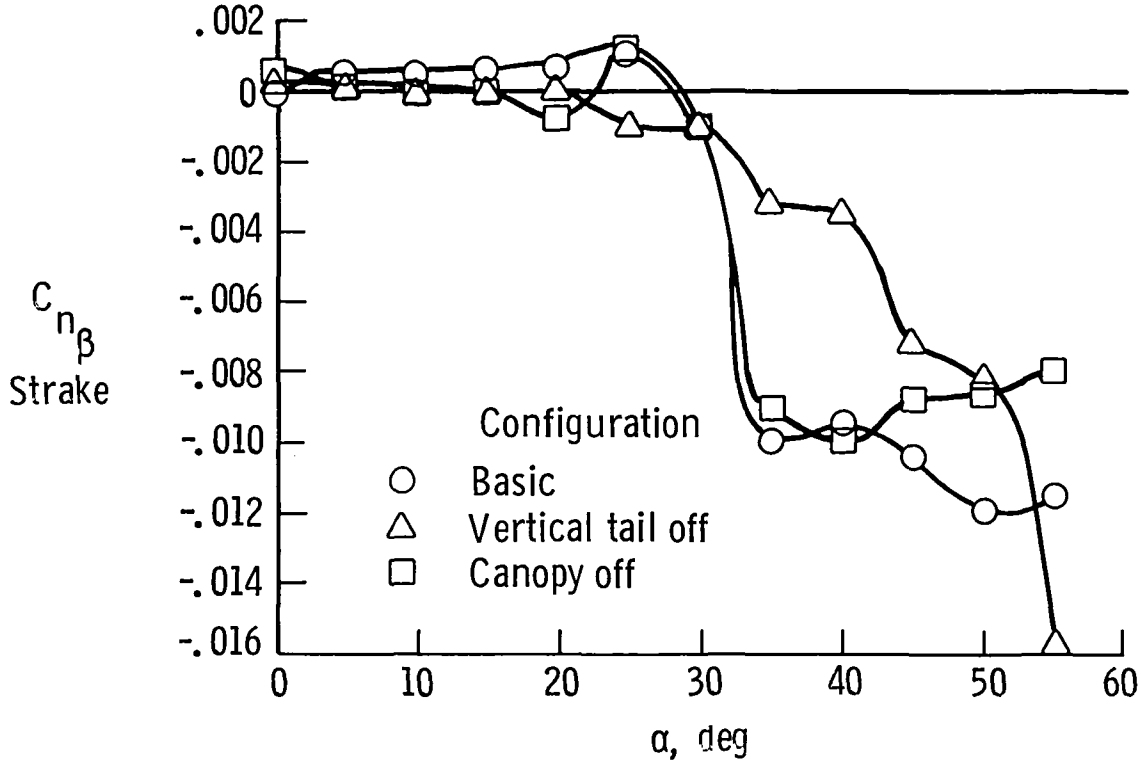

Figure 14. Effect of strake on directional stability for several configurations.

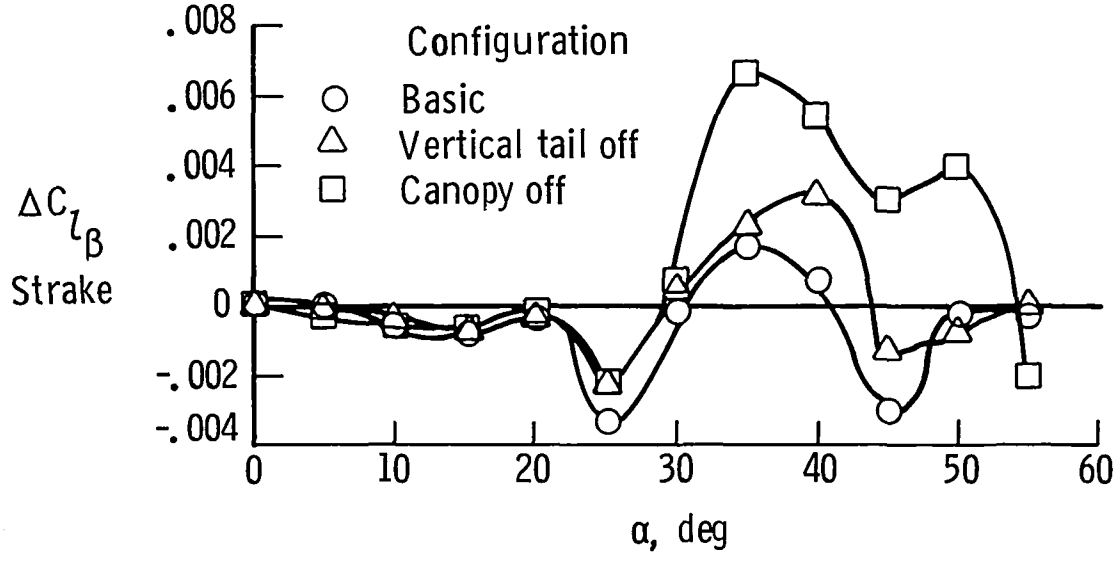

Figure 15. Effect of strake on lateral stability for several configurations.

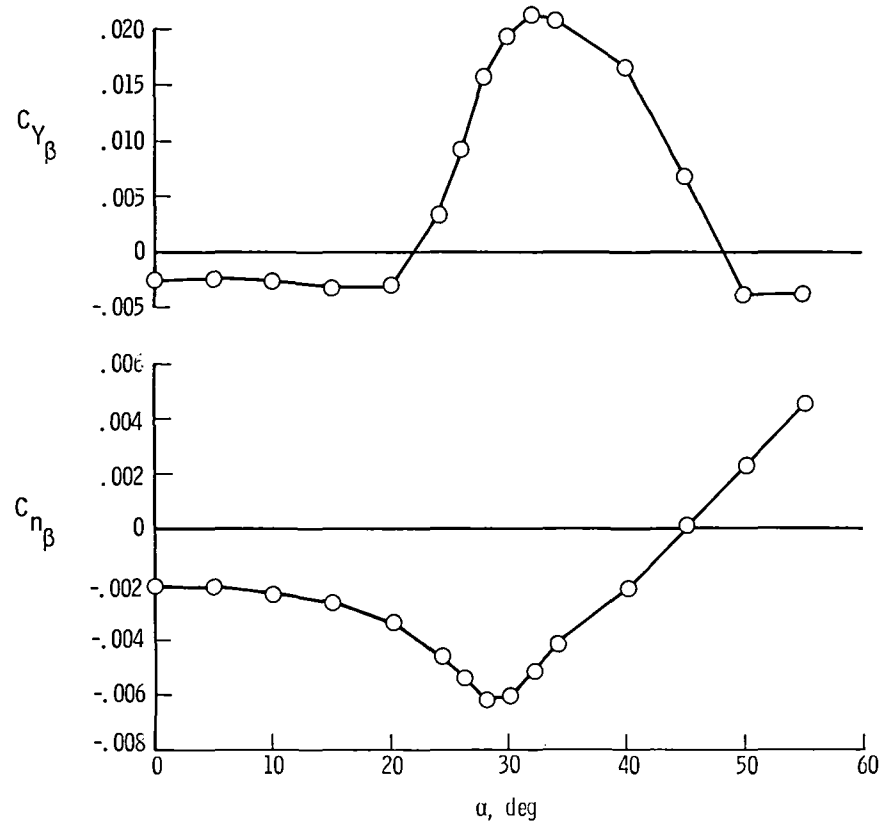

Figure 16. Directional stability derivatives for configuration with body and canopy.

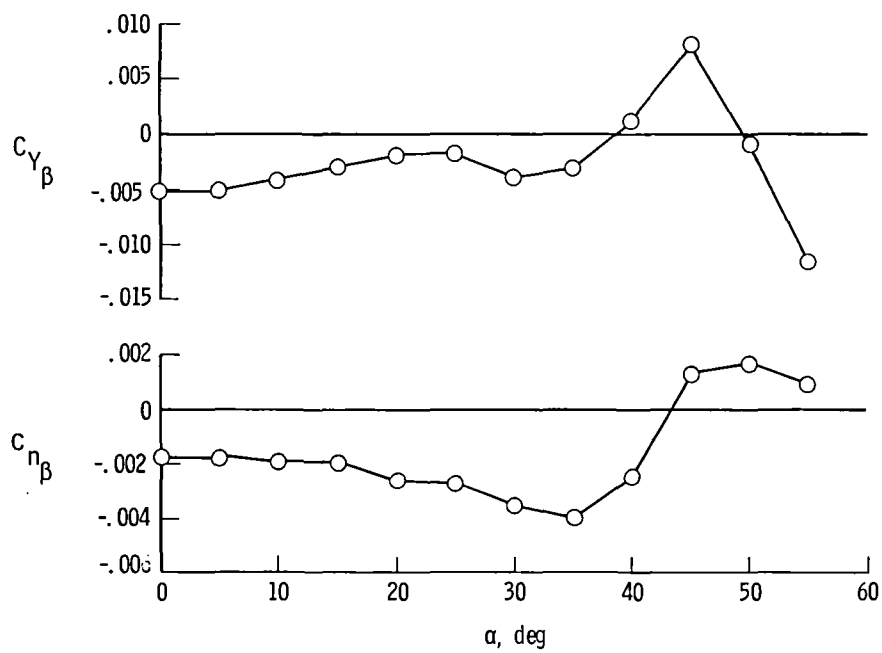

Figure 17. Directional stability derivatives for configuration with body, canopy, and strake.

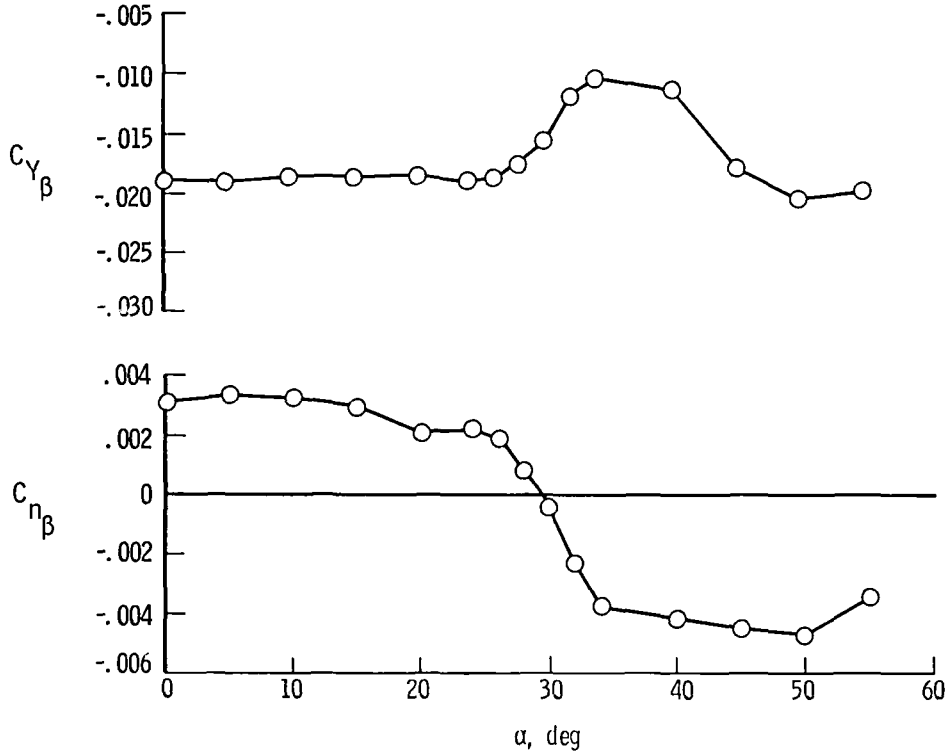

Figure 18. Directional stability derivatives for basic configuration.

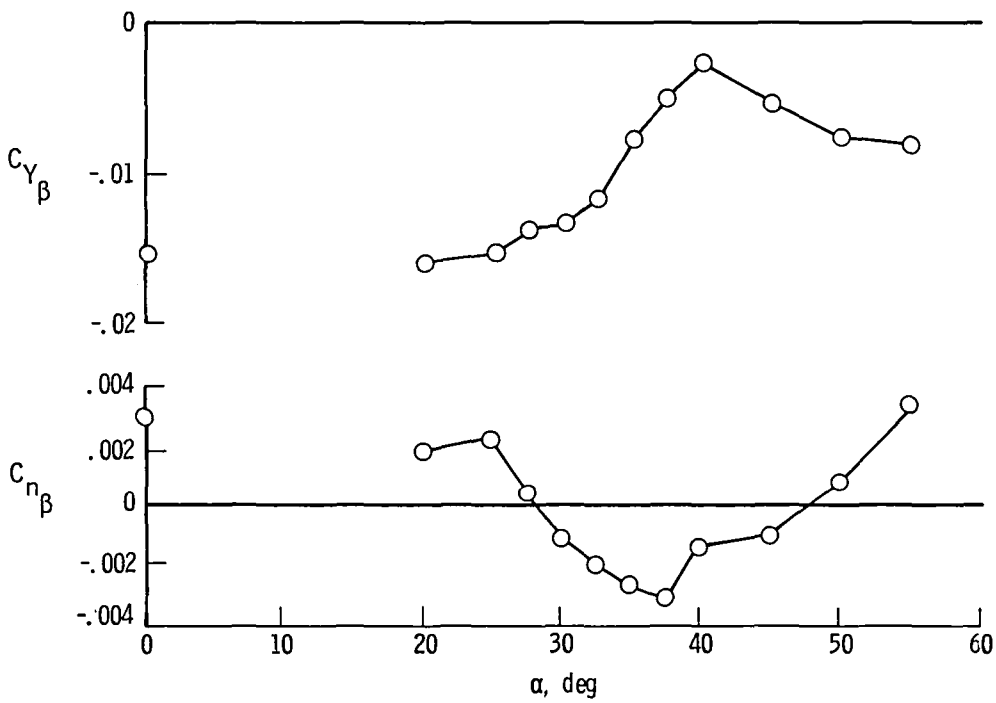

Figure 19. Directional stability derivatives for basic configuration without strake.

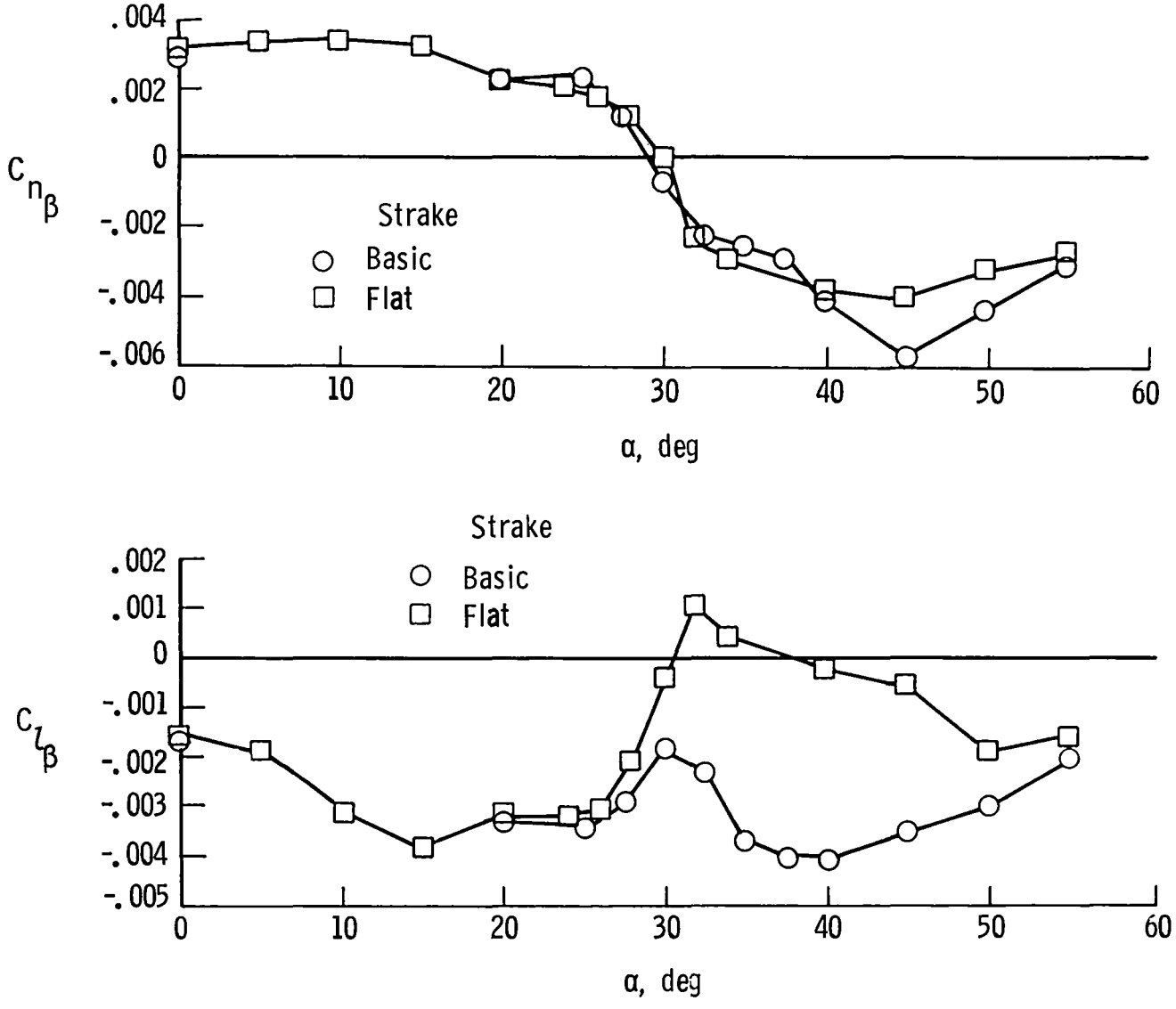

Figure 20. Comparison of directional stability characteristics for model with flat and blended strakes.

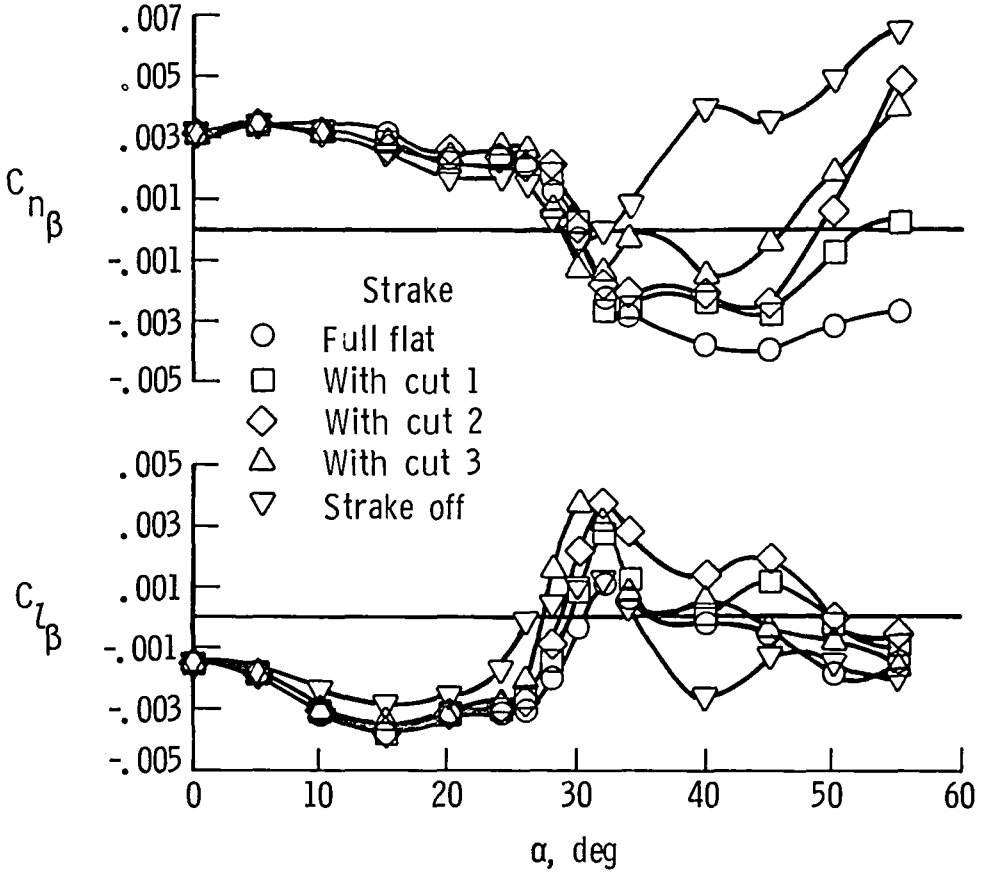

Figure 21. Effect of strake configuration on lateral-directional stability characteristics.

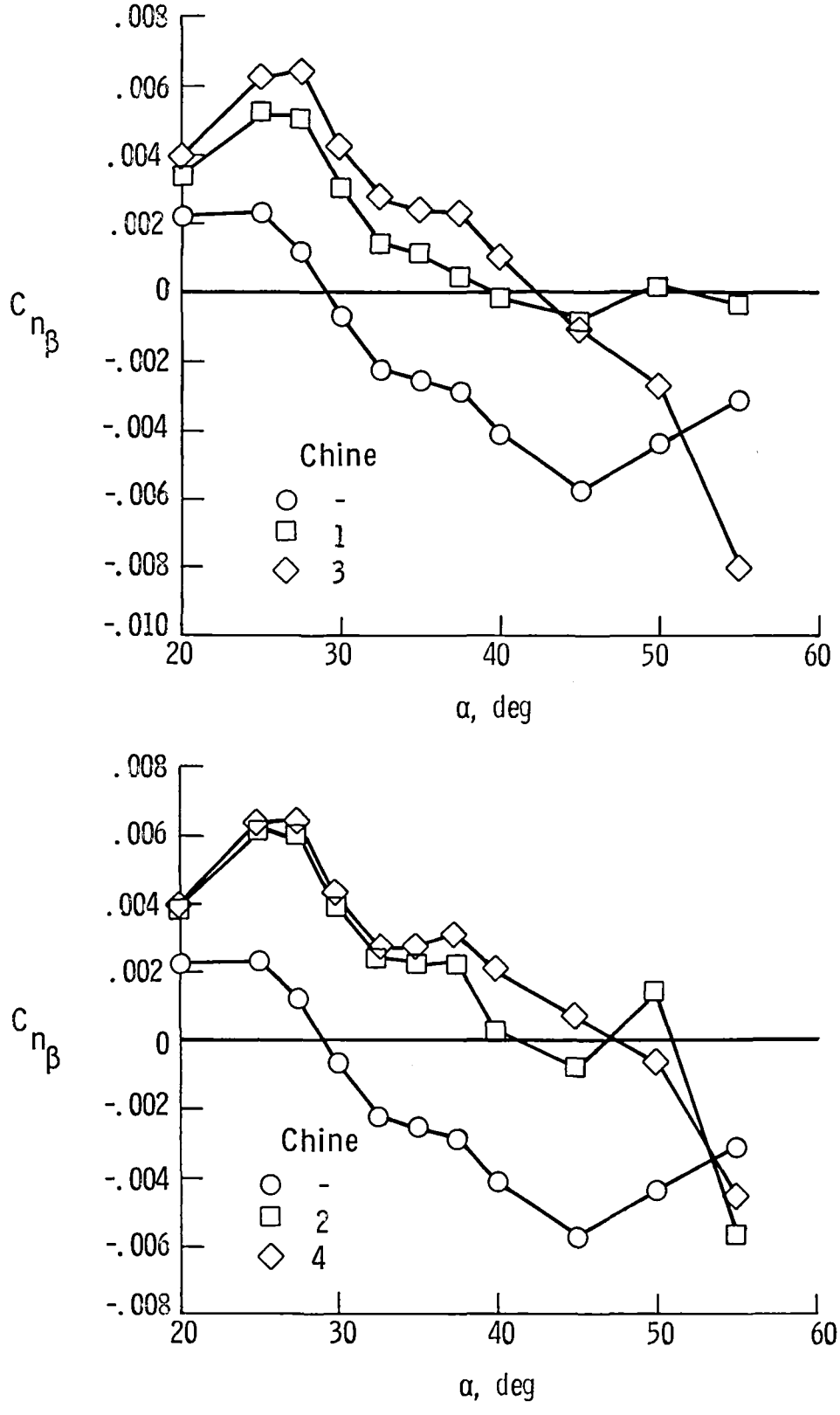

(a) 1.5-in. (full-scale) nose chines.

Figure 22. Effect of nose chines on directional stability.

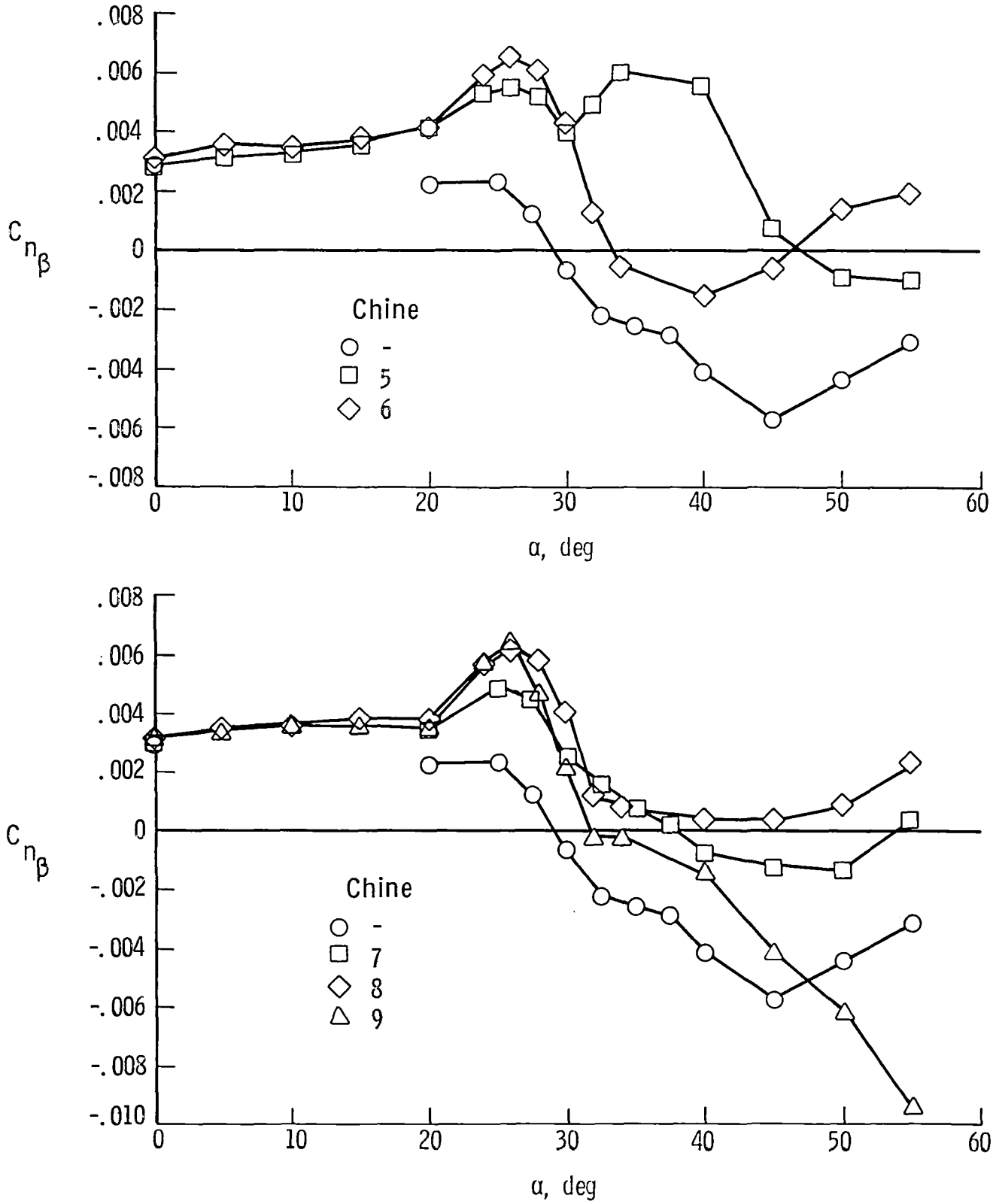

(b) 3-in. (full-scale) nose chines.

Figure 22. Concluded.

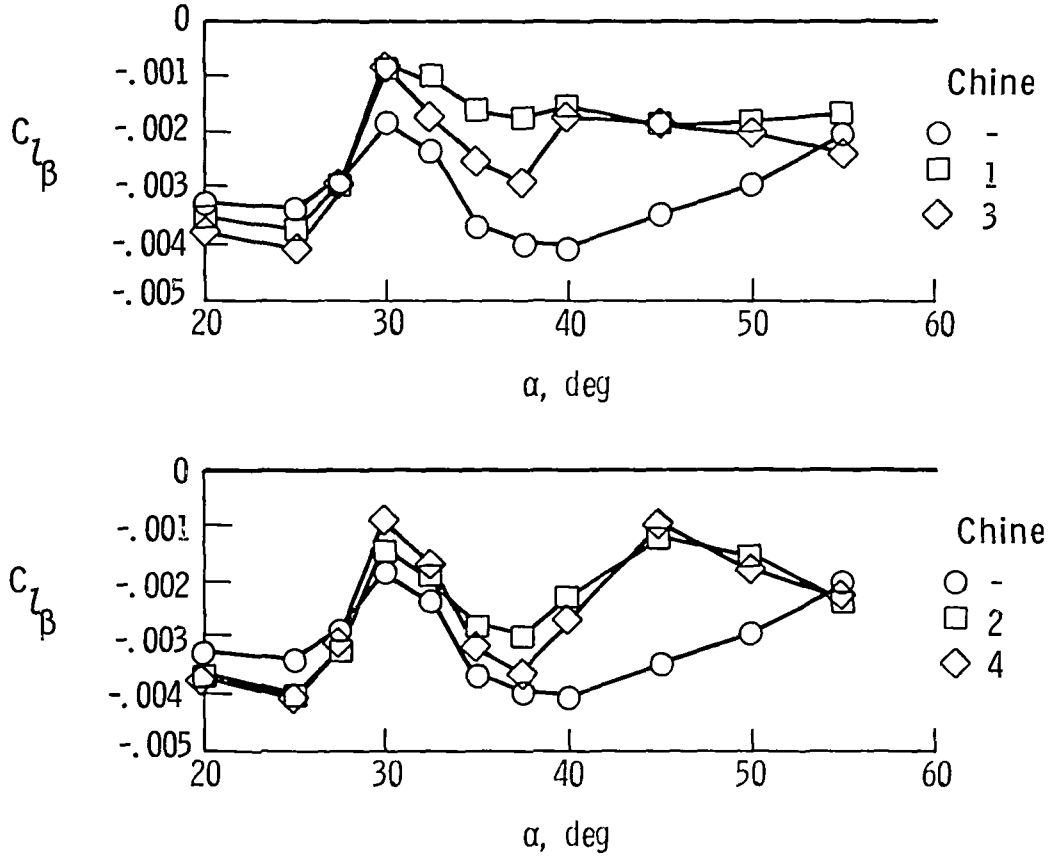

(a) 1.5-in. (full-scale) nose chines.

Figure 23. Effect of nose chines on lateral stability.

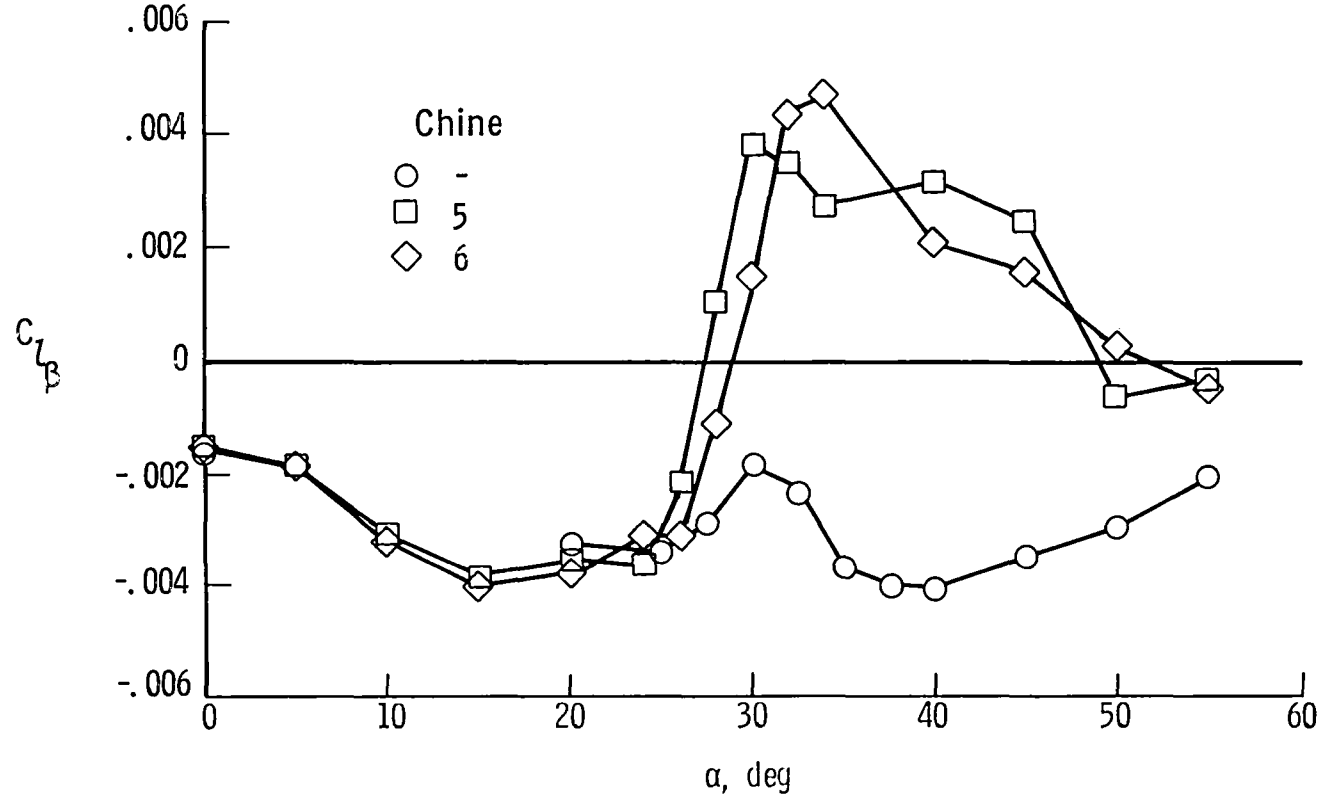

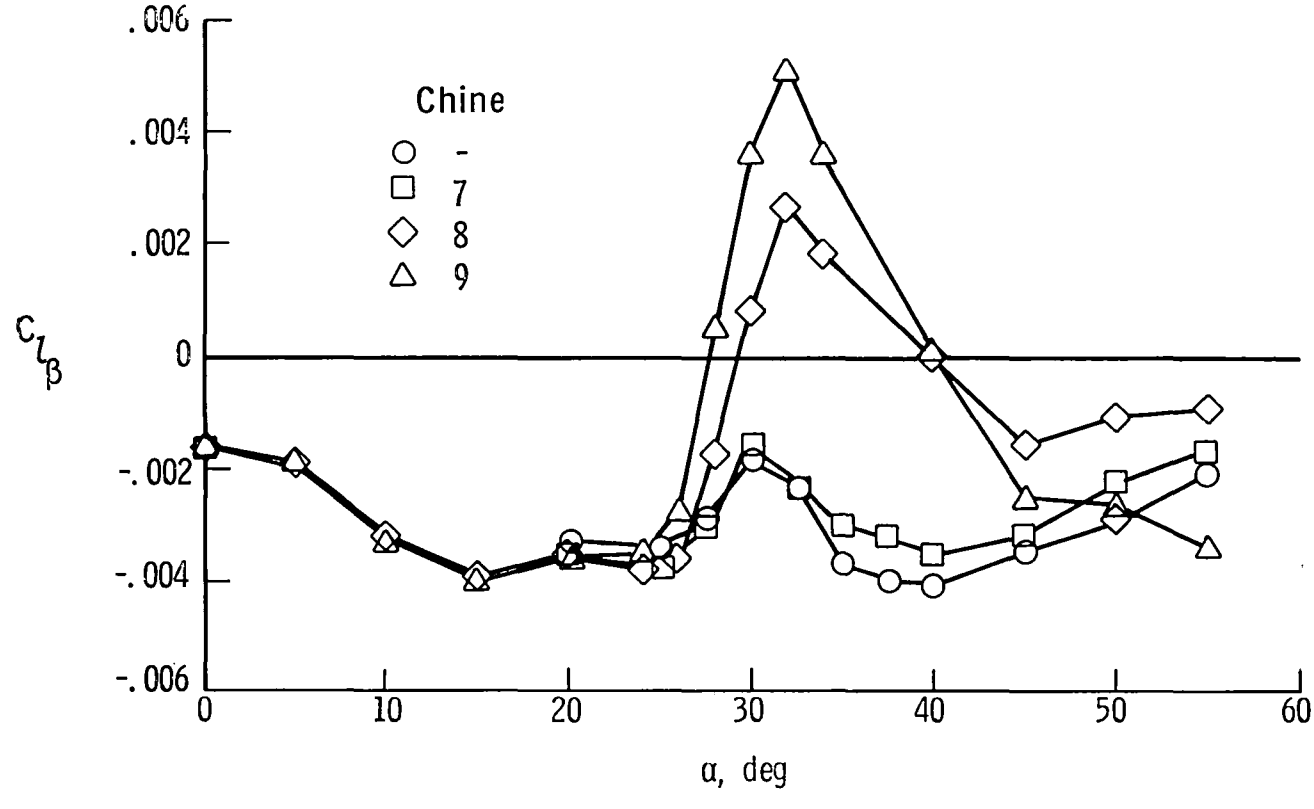

(b) 3-in. (full-scale) nose chines.

Figure 23. Concluded.

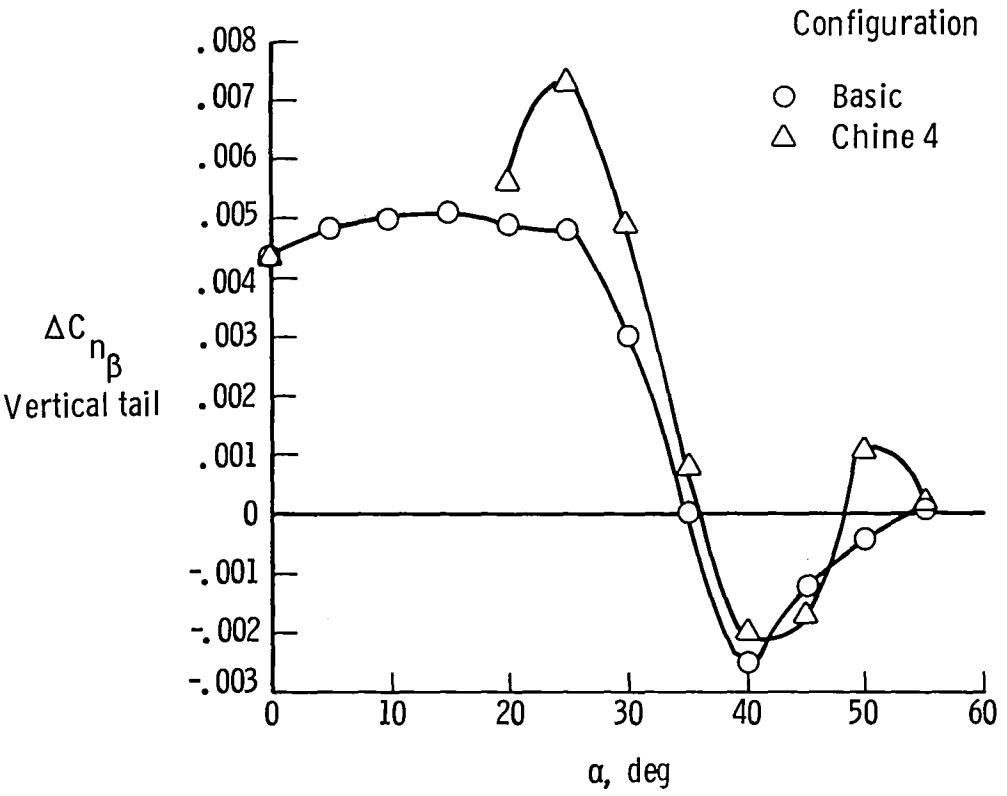

Figure 24. Comparison of vertical-tail effectiveness on directional stability with and without a nose chine.

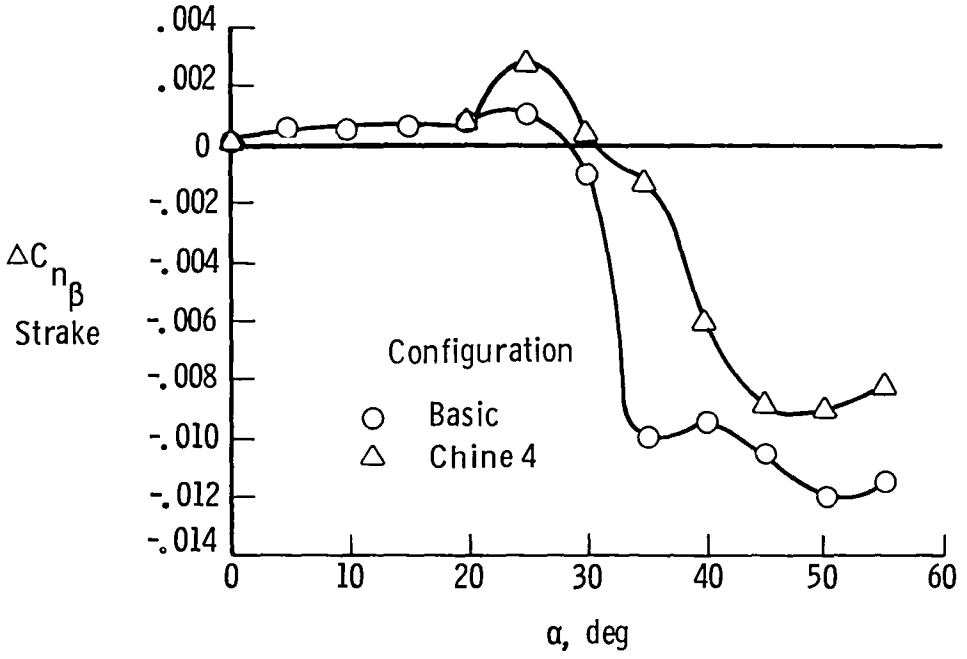

Figure 25. Comparison of strake effectiveness on directional stability with and without a nose chine.

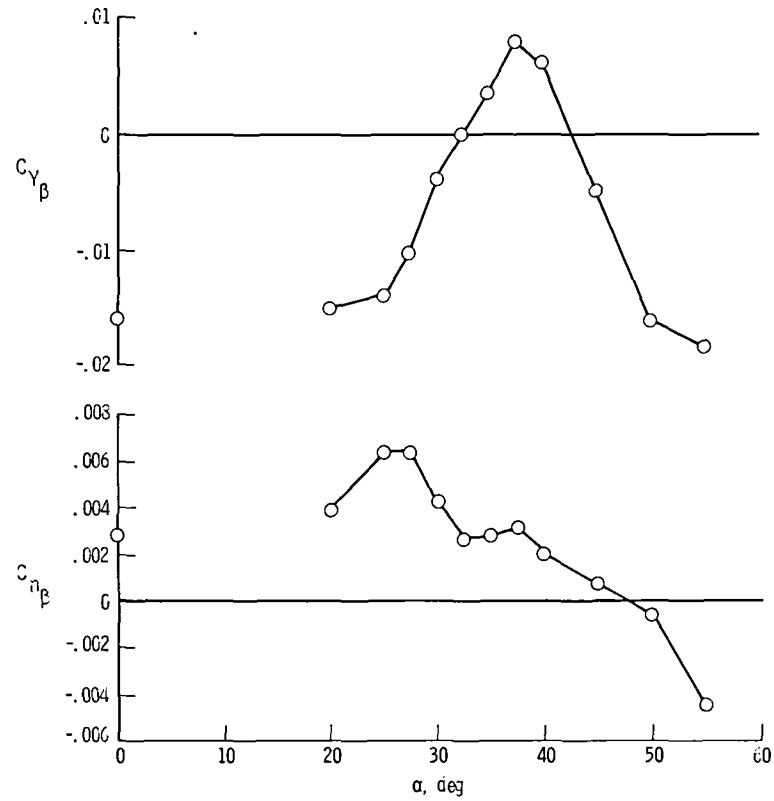

Figure 26. Directional stability derivatives for chine-4 configuration.

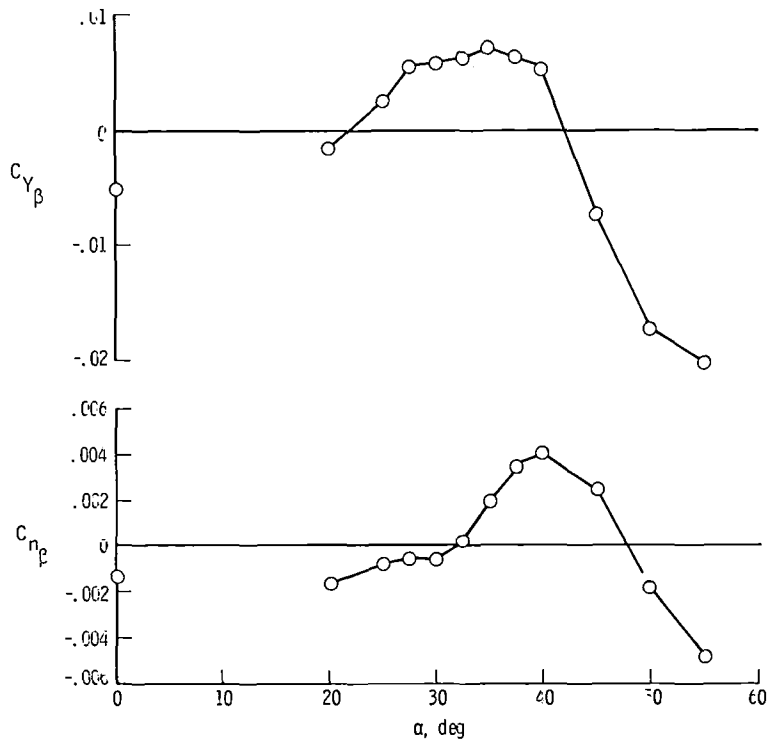

Figure 27. Directional stability derivatives for chine-4 configuration without vertical tail.

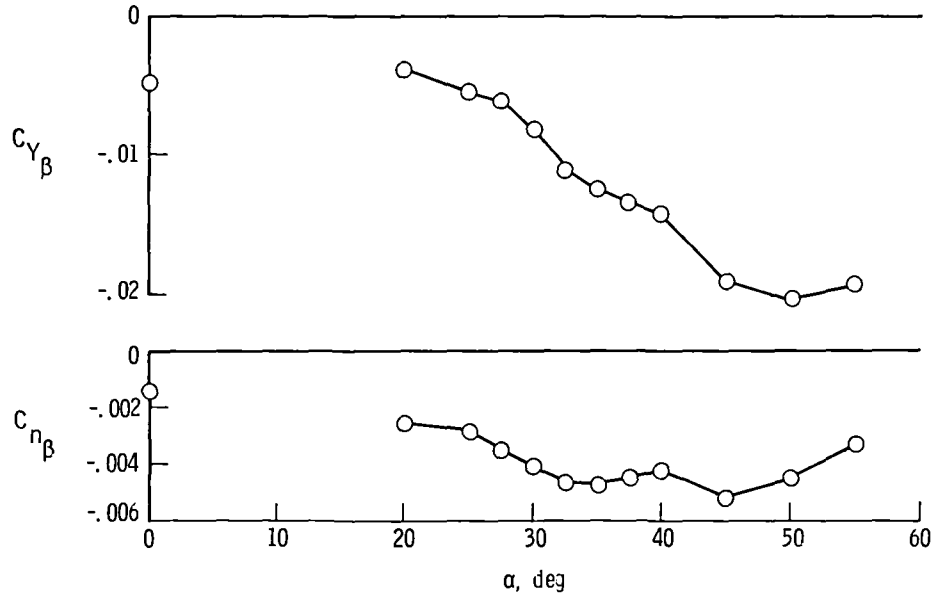

Figure 28. Directional stability derivatives for basic configuration without vertical tail.

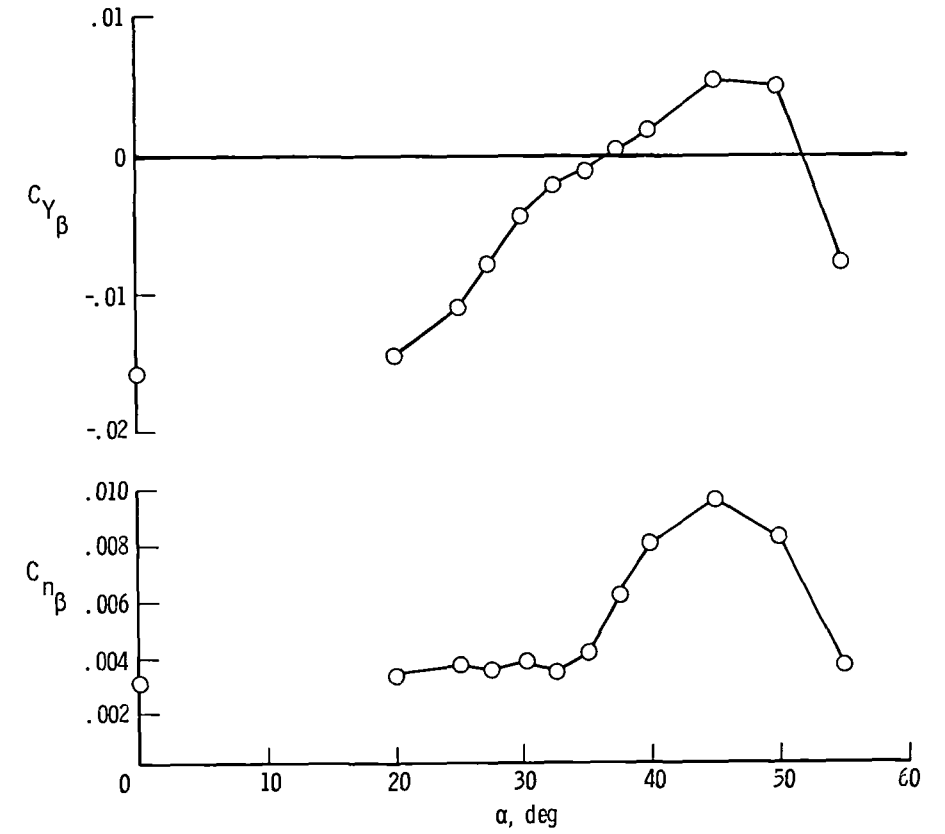

Figure 29. Directional stability derivatives for chine-4 configuration without strake.

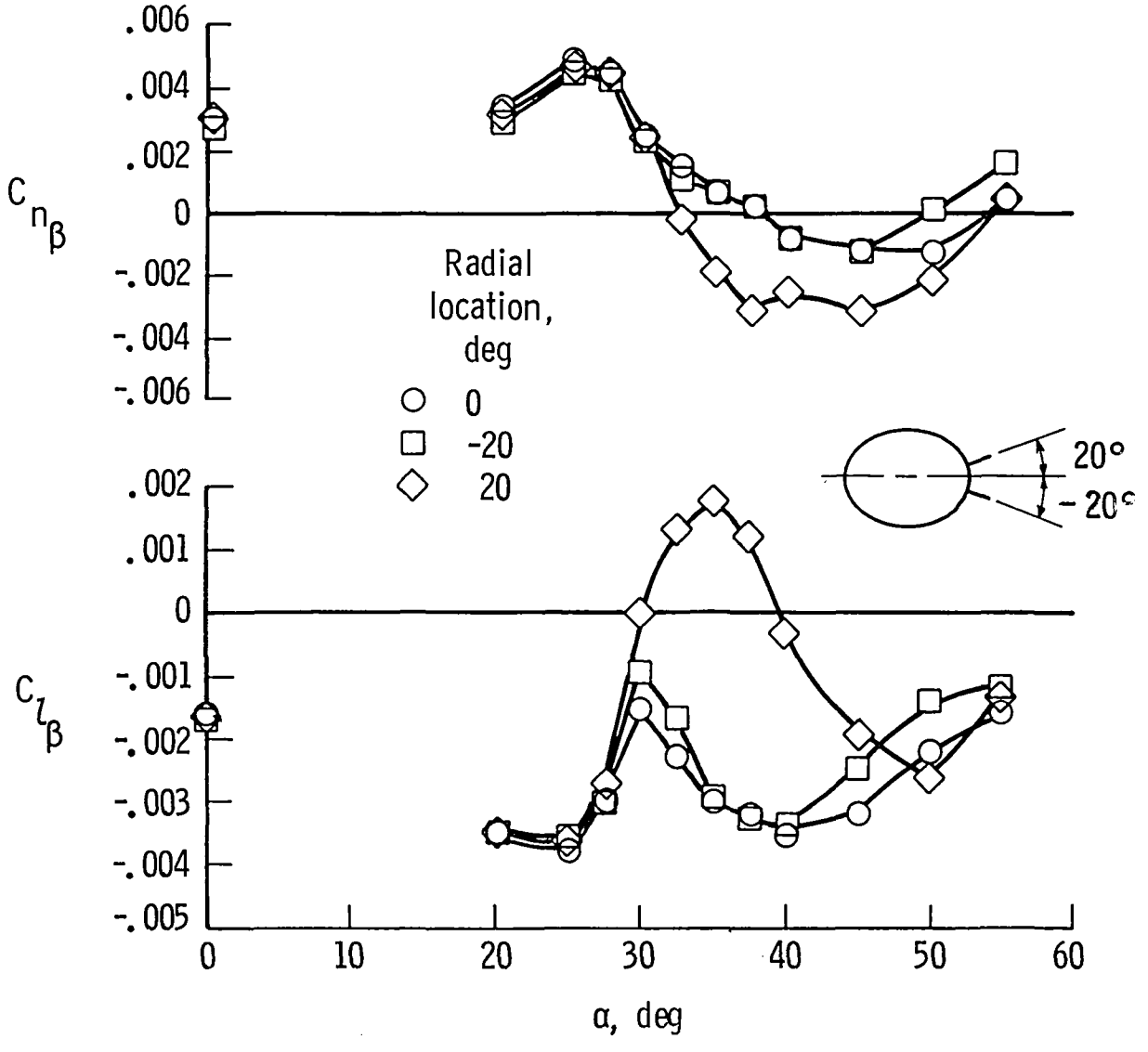

Figure 30. Effect of radial position of nose chine on lateral-directional stability.

1. Report No.	2. Government Accession No.	3. Recipient's Catalog No.
NASA TM-87641		

4. Title and Subtitle	5. Report Date
Low-Speed Wind-Tunnel Investigation of the Effect of Strakes and Nose Chines on Lateral-Directional Stability of a Fighter Configuration	February 1986
	6. Performing Organization Code: 505-43-13-01
7. Author(s): Jay M. Brandon	8. Performing Organization Report No.: L-16051
9. Performing Organization Name and Address: NASA Langley Research Center, Hampton, VA 23665-5225	10. Work Unit No.
	11. Contract or Grant No.
12. Sponsoring Agency Name and Address: National Aeronautics and Space Administration, Washington, DC 20546-0001	13. Type of Report and Period Covered: Technical Memorandum
	14. Sponsoring Agency Code

15. Supplementary Notes

16. Abstract

A series of low-speed static wind-tunnel force tests were conducted on a 0.15-scale model of a modern high-performance fighter aircraft. The tests identified sources of lateral-directional instabilities and investigated the use of nose chines to enhance stability at high angles of attack. Results of this investigation showed that the strake was the major contributor to directional instability. The destabilizing forces were created by two mechanisms: (1) adverse flow in the region of the vertical tail, and (2) forces generated on the fuselage ahead of the center of gravity. Properly designed nose chines effectively negated the adverse flow near the vertical tail and created stabilizing forces on the forebody in the range of the stall angle of attack.

17. Key Words (Suggested by Authors(s))
Strake
Chine
Lateral-directional stability
Longitudinal stability
High angle of attack
Forebody aerodynamics

18. Distribution Statement
Unclassified—Unlimited

Subject Category 02

19. Security Classif.(of this report)	20. Security Classif.(of this page)	21. No. of Pages	22. Price
Unclassified	Unclassified	31	A03

For sale by the National Technical Information Service, Springfield, Virginia 22161

NASA-Langley, 1986

National Aeronautics and
Space Administration
Code NIT-4

Washington, D.C.
20546-0001

Official Business
Penalty for Private Use, $300

BULK RATE
POSTAGE & FEES PAID
NASA
Permit No. G-27

NASA

POSTMASTER: If Undeliverable (Section 158 Postal Manual) Do Not Return